The localization of chitin synthase mediates the patterned deposition of chitin in developing Drosophila bristles.

Paul N. Adler

Biology Department

Cell Biology Department

University of Virginia

Charlottesville, VA 22904

Abstract

The insect exoskeketon is a morphologically complex structure that is a key for the life style of this very successful group of animals. The cuticular cytoskeleton contains proteins, lipids and the N-acetyl glucosamine polymer chitin. Chitin is a highly patterned and essential component of the insect exoskeleton synthesized by chitin synthase. In most body regions chitin fibrils are found in a stack of parallel arrays that can be detected by transmission electron microscopy. Each array is rotated with respect to the layers above and below. In sensory bristles, chitin primarily accumulates in bands parallel to the proximal/distal axis of the bristle. These bands are visible by confocal microscopy providing experimental advantages. We have used this cell type and an edited chitin synthase gene to establish that the bands of chitin are closely associated with stripes of chitin synthase. This argues that the localization of chitin synthase plays an important role in mediating the patterned deposition of chitin in insect cuticle. However, other data suggest this connection may not be absolute. Several genes are essential for proper chitin deposition. We found one of these, *Rab11* is required for the insertion of chitin synthase into the plasma membrane and a second, *duskylike* is required for plasma membrane chitin synthase to properly localize into stripes. We also established that the actin cytoskeleton is required for the proper localization of chitin synthase and chitin in developing sensory bristles. An unexpected finding is that chitin synthase and other membrane proteins are shed during or after the process of cuticle deposition and this may explain cases where there is a lack of a sharp phenotypic boundary between cells that have or lack chitin synthase activity.

Introduction

Chitin is an abundant and widespread extracellular polymer found in many types of eukaryotic organisms from fungi to vertebrates. It is synthesized by the multi-pass transmembrane enzyme Chitin Synthase (CS) and has been most studied in fungi and insects, where chitin plays important structural roles. In fungi chitin is a constituent of the cell wall and the number of CS genes in fungi is quite variable (Merzendorfer, 2011). For example, S. cereviase has 3 CS genes (Gohlke et al., 2017) while Aspergillius fumigatus has 8 (Muszkieta et al., 2014). Chitin in fungal cell walls is not uniformly distributed and in these systems different CS's appear to have different subcellular localizations and to mediate chitin synthesis in different parts of the cell wall including the bud ring (Cabib and Bowers, 1971; Foltman et al., 2018). In insects, chitin is a major component of the cuticular exoskeleton, the apical surface of trachea and the peritrophic membrane that lines the gut (Merzendorfer, 2011). In the cuticle, it is in parallel arrays while in the peritrophic membrane it is a fibrous mesh. There are two CS genes in insects, one functions in the formation of the cuticular exoskeleton and tracheal lining and the other synthesizes the chitin found in the peritrophic membrane (Merzendorfer, 2011). In Drosophila the chitin synthase enzyme required for the synthesis of cuticle chitin is encoded by the *kkv* gene (Moussian et al., 2005; Ostrowski et al., 2002). On the surface, the larger number of CS encoding genes in fungi is surprising as the insect exoskeleton is a morphologically more complicated and varied structure than the fungal cell wall.

The most conserved region in all chitin synthases is the catalytic domain (con1) (Dorfmueller et al., 2014; Nagahashi et al., 1995; Yabe et al., 1998) and this region is essential and sufficient for chitobiose synthesis by SC-CHS2. A second conserved region (con2-ref) is essential for the synthesis of long chito-oligosaccharide, and seems likely to be essential for the translocation of growing chitin chains (Dorfmueller et al., 2014; Yabe et al., 1998). Con1 from SC-CHS2 shows substantially higher sequence conservation than con2, but both can be recognized in insect chitin synthases such as Drosophila Kkv. Both of these regions are thought to be cytoplasmic in yeast CHS2, although there is evidence for two transmembrane domains separating the catalytic site from at least the c terminal most part of Con2 (Gohlke et al., 2017) . The insect cuticle CS is typically larger than most fungal CS proteins. For example, the Drosophila CS1 contains 1615 amino acids while yeast CHS3 contains 1165 amino acids. The larger size might allow the insect protein to interact with a larger number of other proteins and this could be important in the development of the morphological complexity of insect cuticle. All CS are multi-pass transmembrane proteins. The number of inferred transmembrane domains varies from ~5 to 18 with fungal CS proteins generally predicted to contain many fewer putative transmembrane domains than insect CS proteins (Gohlke et al., 2017; Merzendorfer, 2011) (Merzendorfer and Zimoch, 2003). However, since different programs predict different numbers of transmembrane domains for individual CS until direct experimental data provides answers there will be uncertainty (Gohlke et al., 2017). Indeed, in the case of fungal chitin synthases direct experimental data established that the computer programs for predicting transmembrane domains are useful but not able to accurately predict membrane protein topology (Gohlke et al., 2017). We report here experimental evidence that the amino terminus of Drosophila Kkv is in the cytoplasm and the carboxy terminus in the extracellular space.

99 The arrangement of chitin in insect cuticle may differ in different structures. Over most of the cuticle
100 chitin is found in layers of parallel arrays of chitin fibrils with each layer rotated with respect to its
101 neighbors above and below (Bouligand, 1972; Moussian, 2013; Moussian et al., 2006a). As assayed by
102 confocal microscopy, in the cuticle that covers the shaft of sensory bristles chitin is found most
103 abundantly in bands that run parallel to the proximal-distal axis of the bristle (Nagaraj and Adler, 2012).
104 In transmission electron micrographs we did not see evidence for the presence of chitin layers in bristles
105 or in hairs (trichomes), but whether this represents a true difference or is a consequence of a higher
106 density of cuticle proteins masking the layers remains uncertain. In this paper we make use of the
107 bristle shaft as a model cell type to study patterned chitin deposition in insects. The large size of these
108 polypoid cells makes them favorable for this purpose.

109 The insect cuticle Chitin synthase has been particularly difficult to study in vitro and what is known
110 about it and the process of chitin deposition is relatively limited (Merzendorfer, 2011). Chitin fibrils are
111 insoluble at physiological pH (Elieh-Ali-Komi and Hamblin, 2016), which restricts models for how
112 patterned chitin deposition can be mediated at the cellular level (Fig 1A). One possibility is that in
113 insects as in fungi CS is localized in a patterned way to specific membrane domains and chitin deposition
114 is directly patterned by this. In insect epidermal cells rows of elevated membrane called undulae have
115 been proposed to be the site of chitin deposition (Moussian et al., 2007) (Moussian et al., 2006a). The
116 tips of the undulae are associated with extracellular matrix (Moussian et al., 2006a) (Adler, 2017) but it
117 is not clear if this material is composed of chitin, cuticle, other extracellular proteins/carbohydrate or
118 more than one of these. Interestingly, prominent undulae are not seen during the deposition of some
119 chitin containing cuticle, for example the cuticle that covers wing hairs or bristles (Adler, 2017; Sobala
120 and Adler, 2016). Thus, it seems unlikely that undulae per se are essential for cuticle deposition. An
121 alternative model is that the synthesis of chitin is not patterned but that chitin binding proteins bind to
122 chitin fibrils as they are extruded through the membrane and serve as carriers to mediate the
123 movement of the chitin to the correct place in the developing cuticle. There are a large number of
124 proteins encoded by insect genomes that contain a chitin binding domain and could be part of such a
125 system (Karouzou et al., 2007; Willis, 2010) . In such a model, it seems likely that one or more
126 unidentified proteins are first deposited in a patterned way and they interact with the chitin binding
127 protein-chitin complex to guide the location for chitin fibril deposition. A third model is that CS
128 containing exosomes/chitosomes are secreted and these are guided to the correct location for
129 patterned chitin fibril deposition by interactions between exosome membrane proteins and one or more
130 cuticle components. There are suggestions in support of this sort of model in the literature but evidence
131 for exosomes has not been reported in transmission EM studies on cuticle deposition in Drosophila (e.g.
132 (Sobala and Adler, 2016)). However, here we report evidence that Kkv (i.e. Drosophila CS) is shed during
133 or after the synthesis of the pupal cuticle consistent with a possible exosome model. One difference
134 between these models is that the first predicts that *kkv* should act strictly cell autonomously while the
135 second and third models suggest the possibility of limited cell non-autonomy. Previous experiments
136 have described *kkv* as acting cell autonomously (Ren et al., 2005) (Adler et al., 2013) but we show here
137 experimental evidence that can be explained by a small degree of non-autonomy.

138 As noted above the accumulation of chitin in the cuticle of Drosophila sensory bristles occurs primarily
139 in bands parallel to the long axis of the bristle (Nagaraj and Adler, 2012) and we have used this to
140 examine the relationship between the localization of Chitin Synthase (Kkv) to the patterned
141 accumulation of chitin. We find Kkv is closely associated with these chitin bands during cuticle
142 deposition. This is true even when both patterns are highly abnormal. The accumulation of Kkv is not
143 smooth like the chitin bands but is punctate. To clarify the text we use stripes to describe the
144 accumulation of Kkv and bands to describe chitin. We previously identified several genes whose
145 function was essential for the accumulation of bristle chitin in parallel bands (Nagaraj and Adler, 2012).
146 Knocking down the function of two of these genes resulted in a failure of the accumulation of Kkv in
147 stripes. These observations link the patterning of extracellular chitin to the patterning of Kkv
148 localization in the apical plasma membrane of epithelial cells and begin the identification of genes that
149 mediate both the insertion of Kkv into the plasma membrane and the organization of Kkv in stripes
150 along the proximal distal axis of the bristle.

151 We also observed that a putative catalytically inactive Kkv did not localize properly suggesting the
152 possibility that the secretion of chitin is important for either the establishment or maintenance of Kkv
153 localization. A second possibility is that the active site mutation altered the structure of the protein and
154 that led to the abnormal localization.

155

156

157 **Results**

158 **Generation and characterization of transgenes and edited genes that encode tagged Kkv.**

159 As a first step in examining the role of CS localization in the patterning of chitin deposition we generated
160 a series of new genetic reagents consisting of 3 different *UAS-kkv* transgenes and two edits of the
161 endogenous *kkv* gene (Fig 1BC) (see Methods for details).

162 In one of the UAS transgenes the *kkv* open reading frame was tagged on the C terminus by the bright
163 mNeonGreen (NG) fluorescent protein (Shaner et al., 2013) (*UAS-kkv::NG*). In a second it was tagged by
164 the ollas epitope tag (Park et al., 2008) and his_6 (*UAS-kkv-OH*). We also examined a variant of the NG
165 tagged protein that contained the amino acid change found in the amorphic *kkv*-1 allele (R896K)
166 (Moussian et al., 2005). When expressed using *ap-Gal4* as a driver only modest phenotypes were seen
167 were seen with *UAS-kkv::NG* or *UAS-kkv-OH* and these were also seen at a lower frequency in *ap-Gal4*
168 flies that did not contain a *UAS-kkv* transgene. The most distinctive were small regions of melanized
169 cuticle seen primarily near the suture connecting the scutum to the scutellum on the notum (Fig S1).
170 This phenotype is very rare in *ap-Gal4* flies. The basis for this phenotype is unclear as it does not
171 appear to be a straight forward gain of function as an equivalent phenotype is seen *in ap-Gal4/+;*
172 *Df(3R)ED5156/+* flies (Df(3R)ED5156) deletes the *kkv* gene) (Dos Santos et al., 2015; Ryder et al., 2007).
173 Further, the phenotype associated with *ap-Gal4* driven expression of *kkv::NG* was neither enhanced nor
174 suppressed when a copy of *kkv* was deleted. We also observed the loss (or less frequently deformation)

175 of one or more scutellar or dorso-central bristles in these flies and a malformed scutum, but these were
176 also seen to a lesser extent in *ap-Gal4* flies and to a similar extent in *ap>kkv::NG* and *ap-Gal4/+;*
177 *Df(3R)ED5156)/+* flies. It is not surprising that our UAS transgenes do not show dramatic gain of
178 function phenotypes as Moussian and colleagues (Moussian et al., 2015a) have established that Kkv
179 requires a second protein (MH2 domain containing - either Reb or Exp) for the accumulation of chitin.

180 We used CRISPR/Cas9 and Homology Dependent Repair (HDR) to edit the endogenous *kkv* gene to add
181 two different C terminal tails (see methods for details). In one we added the mNeonGreen fluorescent
182 protein (NG) (Shaner et al., 2013) while in the second we added *smFP-HA* (Viswanathan et al., 2015) (Fig
183 1BC), which is a variant of super folder GFP with multiple HA tags inserted into loops of GFP. Both
184 *kkv::NG* and *kkv::smFP-HA* were homozygous viable and showed no mutant phenotypes under a stereo
185 microscope. Homozygous *kkv::NG* flies also showed no morphological defects when we examined
186 mounted cuticle by compound light microscopy or scanning electron microscopy (Fig 2EF, S2CD). This
187 was also true for *kkv::NG/DF* and *kkv::NG/kkv*^{1}. The data establish the edited gene and protein are close
188 to if not functionally equivalent to wild type. When we examined *kkv::smFP-HA* cuticle by SEM or
189 compound light microscopy we detected a mutant phenotype in wing hairs consisting primarily of thin
190 and bent hairs (Figs 2EF, S2A). The phenotype appeared slightly stronger in *kkv::smFP-HA*/*Df* flies but
191 we did not attempt to quantify this (Fig S2AB). In *ap-Gal4; UAS-kkv::NG kkv::smFP-HA/kkv::smGFP-HA*
192 and *ap-Gal4; UAS-kkv::NG kkv::smFP-HA/Df(3R)ED5156* flies the wing hair phenotype was rescued in the
193 dorsal wing cells where *ap* drives expression of *kkv::NG* but not in the ventral wing cells that served as
194 an internal control (Fig 2GH). Similar results were obtained when *UAS-kkv-OH* was substituted for *UAS-*
195 *kkv::NG.* We examined pupae that expressed Kkv::NG and Kkv::smFP-HA by in vivo confocal imaging.
196 The level of fluorescence was much higher for Kkv::NG (we estimate it as being ~15X brighter (see
197 Methods and Fig S3)) and hence we used it for all of the protein localization experiments described
198 below. These data are consistent with *kkv::smFP-HA* being a viable hypomorphic allele of *kkv* where a
199 lower than normal level of protein accumulates. The hair phenotype is likely due to this structure
200 requiring a higher level of chitin for normal morphogenesis.

201

202 **Subcellular Localization of Kkv**

203 We first used the *UAS* transgenes to examine the subcellular localization of Kkv. Kkv::NG localized on
204 the apical surface of the large polytene salivary gland cells of *ptc>kkv::NG* larvae (Fig S4). The large size
205 of these cells makes them favorable for detecting the apical localization. In wing discs of *ptc>kkv::NG*
206 larvae we observed the expected stripe of expression (Fig S5) in the middle of the wing. We did not see
207 any evidence for the secretion of Kkv::NG in these experiments. As an internal positive control, the
208 larvae also expressed a secreted ChtVis-tdTomato chitin reporter (in red) (Sobala et al., 2015). As
209 expected, Cht-Vis could be detected in the extracellular space between the disc epithelium and
210 peripodial membrane cells. The stripe of Kkv::NG was obvious in living wing discs and in fixed wing discs
211 stained with anti-NG antibodies, establishing that these antibodies did not cross-react with endogenous
212 proteins in wing cells. As is elaborated later, similar specificity was observed for *ptc>kkv::OH* using an
213 anti-ollas monoclonal antibody and when we used a rabbit polyclonal antibody (*anti-Kkv-M*) made

214 against a region from the central part of the Kkv protein (aa1097-1246) to stain the stripe of *Kkv::NG*
215 expression in wing discs. In Z sections we observed that Kkv::NG was preferentially localized to the
216 apical surface of the wing disc cells (Fig S5), as expected for a protein involved in the synthesis of a
217 cuticle component and is consistent on observations of others in different contexts (Maue et al., 2009;
218 Moussian et al., 2015; Zimoch and Merzendorfer, 2002). We also examined fixed *ap>kkv::NG* pupal
219 wings where F-actin was stained with Alexa 568 phalloidin and Kkv-NG by anti-NG antibody (Fig 4G-L).
220 As expected for a transmembrane protein Kkv::NG was localized external to the actin filaments found in
221 the center of growing hairs (Fig 4H) (Adler et al., 2013; Turner and Adler, 1998; Wong and Adler, 1993).
222 This close localization is reminiscent of the apical F-actin and chitin in wing hairs (Adler et al., 2013) and
223 in late stages of trachea development in Drosophila embryos (Ozturk-Colak et al., 2016). At this stage
224 when cell flattening and wing expansion is under way, a large disc of F-actin is seen under each hair (Fig
225 4K) (Adler et al., 2013). We did not observe a similar disc of Kkv::NG in such wings (Fig 4J). Thus, we
226 conclude there is not a universal connection between the localization of sub membranous F-actin and
227 Kkv in the juxtaposed membrane (Fig 4K).

228 When expressed in developing bristles by *neur-Gal4*, Kkv::NG accumulated in a manner similar to, albeit
229 a bit less precisely than that seen for the protein encoded by the edited endogenous gene (see below).
230 Most of our localization experiments used the edited endogenous gene to eliminate potential over
231 expression issues. However, for some experiments that required immunostaining the use of the UAS
232 transgenes was valuable as it allowed us to examine younger animals where cuticle deposition had not
233 made immunostaining problematic.

234 The use of the Neon Green (and Ollas-His_6) tag to localize Kkv requires that the tag remains associated
235 with the enzyme to provide a meaningful localization. Since chitin synthases are often cleaved and in
236 some cases this has been linked to enzyme activation (Broehan et al., 2007; Merzendorfer and Zimoch,
237 2003) (Zhang and Zhu, 2013) this is a concern (we have also seen evidence for cleavage of Kkv on
238 Western blots - pna, preliminary results). To test if the tags remained associated with the enzyme we
239 stained pupae where *UAS-kkv::NG* expression was driven by *neur-Gal4* using both a commercially
240 available anti-NG monoclonal and our anti-Kkv-M rabbit polyclonal antibody. We observed a clear co-
241 localization in stripes of puncta along the proximal distal axis in bristles using the two antibodies (Fig
242 3DEF). This establishes that the neon green tag from the fusion protein is an accurate reporter for the
243 Kkv protein. We also carried out similar co-localization experiments on *neur>kkv::OH* pupae and
244 observed a similar co-localization using anti-Ollas and anti-Kkv antibodies (Fig 3 GHI). We found similar
245 results for the accumulation of Kkv::NG in pupal wings and wing hairs when expression was driven by
246 *ap-Gal4* (Fig 3MNO).

247

248 **Localization of Kkv encoded by the edited endogenous gene:**

249 We first examined the accumulation of Kkv::NG from the edited endogenous gene in pupal wings as this
250 tissue is the best characterized for the timing of cuticle deposition and gene expression (Adler et al.,
251 2013; Sobala and Adler, 2016). Previously we found that we could first detect chitin in pupal wings in

252 developing hairs around 42 hr after white prepupae (awp) (Adler et al., 2013). We observed Kkv::NG in
253 developing hairs in living pupal wings at 42, 49 and 58 hrs awp (after white pupae) (Fig 4C). The level of
254 fluorescence was lower in 42 hr hairs than in 49 hr hairs. We could also detect Kkv::NG fluorescence in
255 the apical surface of wing cells with higher levels at cell boundaries. This was a bit surprising since the
256 procuticle is not being made and we have not detected chitin in the wing blade at this time (Adler et al.,
257 2013; Sobala and Adler, 2016). We also examined pupal wings that were younger than 40 hrs awp.
258 Confocal images of such wings did not show any fluorescence when examined under the same
259 conditions as >40 hr wings (Fig 4A). However, in digitally enhanced images we detected the
260 accumulation of Kkv::Ng in what is likely the proximal part of the hair (Fig 4B). In older wings (e.g. 76
261 hr) during the middle of procuticle deposition the apical membrane fluorescence was stronger than at
262 earlier times and we could see the pedestals that the hairs are found on at late stages (Fig 4F) (Sobala
263 and Adler, 2016). As noted above, similar, albeit a bit messier results were obtained when we examined
264 *ap>kkv::NG* pupal wings.

265 We next examined the localization of Kkv::NG in thoracic bristles by in vivo imaging from ~40-80 hr awp.
266 Previously we found that chitin accumulated in bands along the proximal distal axis of thoracic bristles
267 starting around 42 hr awp (Nagaraj and Adler, 2012). The level of Kkv::NG fluorescence in younger than
268 50hr awp bristles was lower than in older bristles. (Fig S6). At both early and later stages Kkv::NG
269 fluorescence had a punctate appearance within an overall pattern of stripes along the proximal distal
270 axis of the bristle (Figs 3A-C, 5K, S5E, S6). In some samples, we observed what appeared to be a pair of
271 relatively closely situated stripes. As development proceeded, the stripes became more complete
272 although they never reached the completeness and smoothness seen with chitin bands. In older
273 animals (>70 hrs) the pattern became somewhat less distinct with more inter-stripe fluorescence (Fig S6.
274 When we examined orthogonal views of bristle image stacks the stripes of Kkv were obvious (Fig 5KL).
275 Unless stated otherwise, in subsequent in vivo imaging experiments, we primarily examined bristles
276 from 50-65 hr old animals as these showed the most striking "stripe pattern". Control experiments with
277 Oregon-R pupae established that the florescence we were observing was due to the edited *kkv* gene and
278 not to autofluorescence (Fig S5C-F).

279 As noted in the introduction the relationship between the patterned deposition of chitin and the
280 localization of CS in insects is not clear. To investigate this we carried out experiments where we
281 localized both Kkv::NG and our chitin reporter (Cht-Vis) in bristles in living pupae (Sobala et al., 2015).
282 The bands of ChtVis differed from those of Kkv::NG by being smooth rather than punctate (Fig 3C-C'').
283 The two patterns however were largely co-aligned in stripes along the proximal distal axis of bristles. In
284 cross section the ChtVis signal was usually exterior to the Kkv-NG signal as expected for chitin being
285 secreted and CS being a transmembrane protein localized to the apical plasma membrane (Fig 5O). The
286 stripe of Kkv::NG was often also offset a bit from the ChtVis signal, which could be a consequence of
287 ChtVis reporting on chitin (an accumulated product) while the Kkv::NG signal represent protein at a
288 particular instance in time. The different cellular location (plasma membrane vs extracellular) and
289 geometry likely contributes to this (Fig S7).

290

291 **The actin cytoskeleton influences the accumulation of Kkv**

292 In several experiments, we explored the relationship between Kkv::NG accumulation and the large
293 bundles of cross-linked F-actin found in bristles (Tilney et al., 1995). These experiments were
294 complicated by the breakdown of the actin bundles, which starts around 43 hr (Guild et al., 2002), and
295 our inability to reliably immunostain bristles older than about 48 hr awp. In our best experiments we
296 examined pupae that were 48hr or younger. An additional complication is geometric and due to Kkv
297 being in the plasma membrane (and the NG in Kkv::NG being extracellular as described below) while the
298 F-actin extends some distance into the cytoplasm (Tilney et al., 1995) (Fig S7). Using an F-actin reporter
299 (Lifeact-Ruby - (Hatan et al., 2011; Riedl et al., 2008) we observed a close connection between the
300 localization of Kkv::NG and the large bundles of F-actin in *neur>lifeact-Ruby; kkv::NG* pupae. The results
301 varied from the two appearing to co-localize to their being slightly offset (Fig 5H-J, H'-J') consistent with
302 the geometry considerations (Fig S7).

303 The large bundles of highly cross-linked actin filaments support the shape of growing bristles and in their
304 absence in $sn^3 f^{36}$ double mutants the resulting bristles are bent, curved, split, shorter and stand more
305 upright than normal (Guild et al., 2002; Tilney et al., 2004; Tilney et al., 1995). In separate experiments,
306 we observed an abnormal distribution of chitin and Kkv::NG in living $sn^3 f^{36}$ double mutants. The robust
307 parallel array of chitin bands and Kkv::NG stripes were severely disrupted (Fig 5AB). Kkv::NG was
308 primarily in the plasma membrane and the chitin appeared to be extracellular so the bundles of F-actin
309 do not appear to be required for the targeting of Kkv to the plasma membrane or for the secretion of
310 either chitin or the chitin reporter. To determine the relationship between the abnormal stripes of
311 Kkv::NG and chitin we examined the distribution of both in the same living bristle. We found the linkage
312 between chitin and Kkv::NG was maintained even in these highly abnormal bristles (Fig 5CDE). We often
313 observed stripes of Kkv::NG on both sides of a band of chitin. We have seen this in normal bristles but
314 by casual observation less frequently.

315

316 **Proteins required for the proper localization of Kkv.**

317 We previously established that Rab11 and exocyst function is required for the deposition of cuticle and
318 the bands of chitin in bristles (Nagaraj and Adler, 2012). Affected bristles become unstable and collapse
319 after the highly cross linked F-actin bundles in developing bristles begin to depolymerize (Guild et al.,
320 2002; Nagaraj and Adler, 2012). To determine if the failure to form chitin bands was associated with a
321 failure to properly localize CS we examined Kkv::NG in thoracic bristles of living *neur-Gal4 Gal80-*
322 *ts/Rab11 RNAi; kkv-NG/kkv-NG* pupae that were shifted to 29.5°C at wpp (white prepupae). When
323 allowed to develop to adulthood these animals showed the extreme stub macrocheatae phenotype
324 described previously (Nagaraj and Adler, 2012). The morphology of the bristles was dependent on pupal
325 age. In the youngest animals examined, the bristles were beginning to show the blebbing characteristic
326 of the early stages of the collapse program (Nagaraj and Adler, 2012). In older animals the collapsed
327 stub bristle morphology was seen (Fig 5G, arrow). The stripes of Kkv::NG were lost and in Z sections we
328 found that the protein was not preferentially localized to the plasma membrane and instead was found

329 in the cytoplasm (Fig 5P). These observations indicate that Rab11 function is required for the proper
330 trafficking of Kkv to the plasma membrane and this can explain the loss of chitin bands in the Rab11
331 mutant (Nagaraj and Adler, 2012).

332 The Zona Pellucida domain containing Dusky-Like (Dyl) protein acts as a Rab-11 effector for chitin
333 deposition in bristles (Nagaraj and Adler, 2012). To determine if Dyl was required for the proper
334 localization of Kkv we examined Kkv::NG in thoracic bristles of living *UAS-dyl-RNAi/+; neur-Gal4*
335 *kkv::NG/kkv::Ng* pupae where Dyl expression was knocked down. The bristle collapse phenotype seen
336 in these bristles is similar that of the Rab11 knock down; albeit slightly weaker as not all macrocheatae
337 show the extreme stub phenotype. We observed these bristles in the blebbing stage and observed the
338 loss of the robust striping pattern of Kkv::NG accumulation (Fig 5F). Kkv::NG in such bristles was
339 primarily seen spread around the plasma membrane (Fig 5Q). The distribution was not uniform but was
340 far from the nicely spaced stripes seen in wild type. The data argue that Dyl is required for the
341 localization of Kkv::NG in stripes but not for its insertion into the plasma membrane. The difference in
342 Kkv::NG localization between the Rab11 and Dyl knockdowns suggests that these two genes and
343 proteins mediate different steps in the localization of Kkv.

344 To complement these experiments we also simultaneously localized Kkv-NG and Dyl in bristles by
345 immunostaining. The stripes of Kkv::NG and Dyl were interdigitated but did not appear to touch (Fig
346 5KLM). As described above and elsewhere (Nagaraj and Adler, 2012) the function of the actin
347 cytoskeleton, Rab11 and *dyl* are required for the normal accumulation of both chitin and Kkv::NG in
348 developing bristles. To determine if the function of the actin cytoskeleton is required for the normal
349 subcellular localization of Dyl in stripes we immunolocalized Dyl in developing sn^3 f^{36} bristles. We found
350 that the normal striped accumulation of Dyl was disrupted in the sn^3 f^{36} bristles (Fig S8AB).

351

352 **Localization of an inactive mutant Kkv**

353 We next addressed the question of whether the catalytic activity of Kkv might impact its subcellular
354 localization by placing a R896K mutation put into *UAS-kkv::NG*. This missense mutation is the same one
355 found in the amorphic kkv^1 allele and is in an invariant site that is part of the enzyme's active site
356 (Dorfmueller et al., 2014; Merzendorfer, 2006; Moussian et al., 2005; Nagahashi et al., 1995). When
357 expressed by *ptc-Gal4* Kkv::NG preferentially localizes to the apical surface of salivary gland cells (Fig
358 S4I), while in comparison Kkv R896K::NG was distributed relatively evenly in the cytoplasm (Fig S4J). At
359 higher magnification we observed Kkv::NG accumulated in what appear to be vesicles (Fig S4I') (The
360 salivary gland cells are packed full of vesicles at this stage). In addition to outline fluorescence we
361 observed puncta of Neon Green fluorescence on the vesicles (Fig S4I', arrow). The mutant protein
362 accumulation appeared different with accumulation either between vesicles or in abnormally shaped
363 vesicles (Fig S4 J'). As noted earlier, Kkv::NG accumulates in wing hairs (Fig 4C-L, S4A) the most apical
364 part of wing epidermal cells. In contrast, Kkv R896K::NG did not accumulate in the hair. Rather, it
365 accumulated relatively evenly in the cytoplasm (it appears to be restricted from the nucleus)) (Fig S4B).
366 This was not due to delayed hair development as when we stained for F-actin using phalloidin we

367 observed the expected hairs with Kkv R896K::NG in the cytoplasm (Fig S4CD). In developing bristles Kkv
368 R896K::NG did not routinely accumulate in proximal/distal stripes as the wild type protein does. Rather,
369 much of the protein was not found on the plasma membrane and there were uneven regions with
370 varying levels of fluorescence (Fig S4E-H). One possibility for the mislocalization is that the mutant
371 protein might be cleaved so that NG was no longer a valid reporter for the enzyme. To test this we
372 immunostained both pupal wings and bristles using both the anti-NG and anti-Kkv-M antibodies.
373 Extensive co-localization of the two staining signals indicated that the NG tag remained a valid reporter
374 for the R896K mutant (Fig 3JKL, PQR).

375

376 **Topology of Kkv**

377 Different programs that predict transmembrane domains give different predictions for the topology of
378 Kkv (see Methods for more information). The predictions differ in terms of the number of
379 transmembrane domains and in the predicted location (cytoplasmic vs extracellular) of different protein
380 regions. For example, the TMPRED program predicts 18 transmembrane domains (TMDs) while
381 TMHMM2.0 predicts 15 TMDs. Among 14 different predictions a set of 14 TMDs were included in 13 or
382 14 predictions. Fig 6B shows the locations of these "consensus predictions". The reagents we
383 generated for other reasons provided us with tools we could use to probe the topology of Kkv. We
384 immunostained *ptc>kkv-OH* (and *ptc>kkv-NG*) wing discs either with or without permeabilization of the
385 plasma membrane with Triton X-100 (Fig 6A). We found both anti-NG and anti-Ollas antibodies stained
386 wing discs in the absence of permeabilization indicating that the C terminus is exposed to the
387 extracellular space (Fig 6A). All of the topology programs predicted this. In contrast when we used an
388 anti-Kkv polyclonal antibody (anti-Kkv-M) raised against aa 1097-1246 we did not see any staining in the
389 absence of Triton X-100 permeablization (Fig 6A), arguing this region is intracellular. This disagrees with
390 the consensus prediction. Similar results were obtained when we used antibodies directed against aa
391 53-66 and also antibodies directed against aa 530-541 – a region located not far from the catalytic
392 domain (Fig 6AB). These results indicate that these regions of Kkv are also located in the cytoplasm. It is
393 worth noting that no programs predicted a transmembrane domain in the region encompassing aa 1-53,
394 which when combined with our data suggests that the amino terminus of Kkv is located in the
395 cytoplasm. None of the programs predict a transmembrane domain between the aa 530 and the
396 catalytic domain suggesting this region is part of the same cytoplasmic loop. Our experimental data
397 does not agree with the consensus TM predictions as they suggest that the region between 1097-1246 is
398 extracellular but an antibody directed against this region was unable to stain the protein in the absence
399 of Triton X-100 treatment. No differences were seen when we ran several of the computer analyses
400 with the different Kkv protein isoforms.

401

402 **Kkv is shed**

403 In experiments where we imaged Kkv::NG in living pupae we noticed fluorescent puncta in the
404 extracellular space between the pupal cuticle and the epidermal cells that were in the process of

405 synthesizing the adult cuticle (Fig 3B, S3AB, Fig S9A). To investigate this in more detail we obtained
406 large Z stacks that extended from the pupal cuticle to below the apical surface of the epidermal cells.
407 Pupal cuticle in 50 hr pupae shows substantial autoflourescence so we examined and compared *Ore-R*
408 and *kkv::NG* pupae to determine what if any fluorescence was due to the presence of the Kkv-NG
409 protein. The autofluorescence of the thoracic pupal cuticle of Ore-R was spatially relatively even (Fig
410 7D). In contrast, the fluorescence of pupal cuticle of kkv-NG flies was much more uneven with both
411 puncta (arrow) and lines (arrowhead) of bright fluorescence (Fig 7A). No fluorescence was observed in
412 the region between the pupal cuticle and the apical surface of the epithelial cells in Ore-R pupae (Fig
413 7E). In contrast, in this region many fluorescent puncta were observed in *kkv::NG* pupae (Fig
414 7BC)(arrow). A majority of these were located close to the pupal cuticle but some were observed
415 throughout the region. Most of the puncta located close to the pupal cuticle were stable but many of
416 those located lower were mobile (movie S1). Since the fluorescent puncta were only seen when the
417 *kkv::NG* gene was present we interpret the puncta as evidence of shed Kkv::NG. Since the puncta were
418 located above the impermeable adult cuticle (which is in the process of being synthesized), it seems
419 likely that the Kkv::NG was shed during or after the synthesis of the pupal cuticle and before the
420 synthesis of the adult cuticle began. Consistent with this hypothesis we observed puncta in 28hr pupae,
421 well before the start of adult cuticle deposition (Sobala and Adler, 2016). We also observed puncta in
422 very young pupae (20 hr awp) prior to the detachment of the epithelial cells from the pupal cuticle (Fig.
423 S9B). We observed similar puncta when we examined *ap>kkv::NG* pupae (Fig S9C) but not from *ap>kkv-*
424 *R896K*::NG pupae (Fig S9D), suggesting that to be shed Kkv needs to be localized apically.

425 The highest concentration of puncta were over the dorsal thoracic midline (Fig S9AB). There were also a
426 large number of puncta over the dorsal abdomen and they were seen at a lower frequency in the wing,
427 legs and head. In the abdomen the puncta tended to align parallel to the segment boundary.

428 All of the experiments where we detected puncta in living pupae required imaging of the Kkv::NG fusion
429 protein. Experiments described earlier established that NG was a valid reporter for Kkv in bristles so it
430 seemed likely that it was also a valid reporter for Kkv in puncta. In an attempt to test if this was correct
431 we immunostained pupal cuticle using both anti-NG and anti-Kkv-M antibodies. Among the puncta
432 detected 69.7% stained with both antibodies indicating most puncta contained both NG and Kkv (Fig
433 S10, arrows).

434 The shedding of Kkv::NG could be specific for Kkv or it could reflect a process that leads to the shedding
435 of many if not all of the proteins located in the apical plasma membrane. To distinguish between these
436 two possibilities we examined live *ap-Gal4/+; UAS-mCD8-GFP*/+ pupae. These animals showed a large
437 number of fluorescent puncta present in the space between the pupal cuticle and the apical surface of
438 the epithelial cells (Fig 7GHI). As was the case for the puncta in *kkv::NG* pupae many of the puncta were
439 mobile (movie S2). We conclude that the shedding of membrane proteins is not specific for Kkv or
440 proteins involved in cuticle deposition.

441

442

443 **Cell autonomy of kkv**

444 We previously observed clones of *kkv* in the wing where they lead to faint and flaccid wing hairs (Ren et
445 al., 2005). By examining the morphology of the hairs, the clones appeared to be completely cell
446 autonomous. However, in adult wings the hair is located over the center of the cell and it is not clear if
447 we could detect limited partial cell non-autonomy in such an assay. Given the close juxtaposition of the
448 epidermal cells and the cuticle during cuticle deposition it seems unlikely that CS containing vesicles, if
449 they exist, could diffuse far. To determine if we could detect any evidence of non-autonomy for *kkv* we
450 needed an assay that allowed us to identify *kkv* clones and examine them at a higher resolution than is
451 possible in the light microscope. We found that we could fracture adult cuticle and by scanning
452 electron microscopy detect a layered structure. The layers were very distinctive in abdominal cuticle
453 (Fig S2G) consistent with the robust layering in abdominal procuticle seen by TEM (Fig S2H). We also
454 examined wings attached to studs in a vertical position, fractured and imaged by scanning electron
455 microscopy. In wing cuticle we could also detect a layered structure that presumably reflects the
456 banding of chitin in the procuticle (Fig 8C). The layering was less distinctive than in the abdominal
457 cuticle, which we also found to be true by TEM. We next fractured and observed wings carrying *kkv* loss
458 of function clones. We were able to identify mutant clones by the presence of the *kkv* flaccid hair
459 phenotype (Fig 8DE arrows) (Ren et al., 2005). If there was complete cell autonomy we predicted a
460 sharp change in wing cuticle thickness at wt-mutant clone boundaries (Fig 8A). In contrast, if there was
461 a small degree of cell non-autonomy we predicted that we would see a smooth change in cuticle
462 thickness near the edge of clones (Fig 8A). In all of the clones (n=9) we examined there was a smooth
463 transition in cuticle thickness (Fig 8DE). This transition zone appeared to be restricted to a mutant cell
464 and its direct neighbor.

465

466

467 **Discussion:**

468 **The patterning of Chitin deposition is linked to the localization of Kkv**

469 Our observations generally support a model where the localization of chitin deposition is closely linked
470 to the localization of Kkv (Chitin synthase). The most compelling data being that the localization of
471 chitin and Kkv remain linked even when the distribution of both is abnormal. A limitation of our
472 observations is that they focused on the bands of chitin seen along the proximal distal axis of developing
473 sensory bristles. The cuticle that covers the sensory bristles differs in two ways from the cuticle that
474 covers much of the fly's body. First we have not detected the layering of chitin in TEM studies of bristles
475 although this could simply be due to a higher concentration other components in the procuticle
476 interfering with our ability to detect the layering. A second difference is that the prominent undulae
477 seen in most cells synthesizing cuticle were not detected in bristle forming cells (Adler, 2017). Further
478 studies will be needed to determine if the close connection between chitin and chitin synthase is a
479 general result for arthropod epithelial cells, but that seems likely. The close connection between the
480 two is similar to that seen in yeast and fungi (Leal-Morales et al., 1994) (Chuang and Schekman, 1996)

481 (Santos and Snyder, 1997) (Kozubowski et al., 2003) (Latge et al., 2005) and is reminiscent of the
482 connection between cellulose and cellulose synthase in plants (Polko and Kieber, 2019).
483
484 Our SEM analysis of *kkv* mutant clones showed that there was a gradual thinning of the procuticle in the
485 region where mutant and wild type cells were juxtaposed. That result is not predicted by the model
486 where Kkv in the plasma membrane is localized closely to the deposition of chitin. It better fits the
487 models where either a carrier protein moves chitin fibrils to the site of deposition or secreted vesicles
488 can move a short distance to deposite chitin fibrils over part of a neighboring cell. It is uncertain how to
489 resolve this discrepancy. One possibility is that the biological reality is complicated and chitin synthase
490 is localized but some enzyme or chitin is secreted and can provide chitin fibrils to a neighboring cell.
491 Another possibility is that the gradual change in cuticle thickness is not directly related to a different
492 amount of chitin fibrils but that mechanical forces that are part of wing maturation lead to a smooth
493 transition between the cuticle above neighboring mutant and wild type cells.
494
495 The localization of Kkv in bristles requires both the intracellular transport of the protein into the plasma
496 membrane and its restriction to stripes. In principle, one or two (or more) genetic pathways could
497 mediate these steps. We previously identified the *Rab11* and *dyl* genes as being essential for the normal
498 deposition of chitin in bands in bristles (Nagaraj and Adler, 2012). We found in this paper that in the
499 absence of *Rab11* function Kkv::NG failed to localize to the plasma membrane. In contrast, in the
500 absence of *dyl* function Kkv::NG localized to the plasma membrane but it did not preferentially
501 accumulate into the appropriate stripes. These results argue that there are at least two separate
502 genetic pathways/functional systems that are essential for the localization of Chitin Synthase in insects.
503 The role of *dyl* is of particular interest. Dyl is a ZP (zona pellucida) domain protein and like other ZP
504 domain proteins it can polymerize (Jovine et al., 2005) (Adler et al., 2013; Jovine et al., 2002) and it is
505 thought that through this it can organize the apical extracellular matrix (Chanut-Delalande et al., 2012;
506 Fernandes et al., 2010). The expression of *dyl* is almost entirely restricted to the period of envelop
507 deposition (Sobala and Adler, 2016) and it accumulates in bands along the proximal distal axis of
508 developing bristles (Nagaraj and Adler, 2012). Hence, it localizes in a way that is appropriate for
509 instructing the accumulation of Kkv in stripes. We observed that the stripes of Kkv::NG and Dyl were
510 interdigitated and did not overlap. I suggest that that Dyl functions as a negative factor to prevent the
511 accumulation of Kkv::NG from regions of the bristle plasma membrane, but it may not do so directly as
512 there appears to be space between the interdigitated bands. Future studies will be needed to elucidate
513 the mechanisms involved here (e.g. local Dyl could recruit a factor that removes Kkv::NG from nearby
514 regions of the membrane). In addition to Rab11 and Dyl we also established that the large bundles of
515 cross linked F-actin in bristles were also required for the normal deposition of chitin bands. The
516 localization of both Dyl and Kkv::NG were altered in developing *sn f* bristles. The mislocalization of Dyl
517 provides a mechanism for the mislocalization of Kkv::NG and the subsequent abnormal chitin deposition
518 in these bristles. A number of other genes have been identified that are required for normal chitin
519 deposition or where a loss of function leads to a *kkv* like wing hair phenotype (Adler et al., 2013;
520 Chaudhari et al., 2011; Moussian et al., 2015; Moussian et al., 2006b). It will be interesting to determine
521 if any of these also mediate Kkv localization.
522

523 It is possible that Kkv is actively cycled from the plasma membrane to cytoplasmic
524 endosomes/chitosomes and then back to the plasma membrane. There is strong evidence for the
525 recycling of chin synthase in yeast (Hernandez-Gonzalez et al., 2018; Knafler et al., 2019; Sacristan et al.,
526 2013) and Rab11 is a well-established marker for late endosomes (Calero-Cuenca and Sotillos, 2018)
527 (Welz et al., 2014) and the recycling of membrane proteins. In such a model the failure of Kkv::NG
528 localization in Rab11 deficient bristles could be due to a defect in recycling and not in the original
529 localization. This might also explain the failure of the presumptive catalytic defective Kkv-R896K mutant
530 protein to localize to the plasma membrane. It is possible that the inactive protein is more rapidly
531 removed from the membrane and that it is preferentially not recycled back to the plasma membrane or
532 recycled more slowly. This could be a quality control mechanism in the formation of insect cuticle.

533

534 **Kkv::smGFP is useful as a system for structure function studies on CS.**

535 The importance of chitin synthase function for insects is demonstrated by the lethality associated even
536 with relatively small clones of *kkv* mutant cells (Ren et al., 2005) (Adler et al., 2013) and knocking down
537 *kkv* function for a restricted period of time in a limited set of epidermal cells (pna - unpublished). The
538 edited *kkv::smFP* allele is the only homozygous viable hypomorpic allele of *kkv* that we are aware of. As
539 we demonstrated the rescue of the wing hair phenotype of *kkv::smFP* is an easy assay for testing the
540 functionality of mutant Kkv proteins. This assay relies on UAS-Gal4 driven expression and this could be
541 misleading as overexpression could allow reduced activity mutations to be judged as active. There are
542 however, advantages to this assay compared to editing the endogenous gene. It is important to
543 consider that while CRISPR/Cas9 mediated editing is not difficult it still involves more time and labor
544 than UAS transgenesis and mutations identified as interesting by the UAS-Gal4 system can later be
545 assessed using CRISPR/Cas9 to test for reduced but still significant chitin synthase activity. Further,
546 chitin synthases are known to function as multimers (Merzendorfer, 2011) (Gohlke et al., 2017) and
547 some mutations might be dominant negatives and these could be identified using the UAS-Gal4 system
548 but they would likely fail to be recovered by CRISPR/CAS9 mediated editing (or by classical mutagenesis)
549 as they are likely to be dominant lethals. The UAS/Gal4 system could also be used to identify parts of
550 the Kkv protein that are essential for its localization.

551 It was not surprising that the *kkv R896K* mutant showed no rescue activity as this missense mutation is
552 considered an amorphic allele in Drosohila (Moussian et al., 2005) and a similar substitution in yeast
553 contained only about 1% of wild type activity (Nagahashi et al., 1995). The failure of Kkv R896K to show
554 rescue activity validates this system for structure function studies on the fly CS. It was surprising that
555 this mutant protein did not localize properly. It is possible that the active site missense mutation
556 disrupts both catalytic activity and normal protein folding and the folding defect leads to a failure to
557 traffic the protein to the apical plasma membrane. As noted above it is also possible that the defect is
558 not in the initial trafficking but is due to the inactive protein being recycled more quickly. Further
559 studies will be required to distinguish between these hypotheses.

560 The *kkv::NG* and *kkv-smFP* edits were in the same location in the genome so it is likely that the greater
561 activity and fluorescence of the *kkv::NG* edit compared to the *kkv-smFP* edit is not due to differences in
562 transcription. Rather it is more likely due to the NG tagged protein being either more active and/or
563 accumulating to a higher level than the smFP tagged protein. One possible cause of this is the presence
564 of multiple copies of the HA epitope tag in smFP. A study in yeast reported that a 3XHA tag could cause
565 a dramatic decrease in the accumulation of some of the tagged proteins (Saiz-Baggetto et al., 2017). It is
566 possible that a similar phenomenon can explain our results with *kkv-smFP*.

567

568 **Significance of Kkv shedding?**

569 The shedding of membrane proteins is not a rare phenomenon (e.g.(Lichtenthaler et al., 2018; van Niel
570 et al., 2018)). In most cases the shed material is an ectodomain that is released due to proteolysis
571 (Lichtenthaler et al., 2018). Such a shedding mechanism could explain the shedding of the NeonGreen
572 component; however, it cannot explain our observation that most puncta stained with both an anti-NG
573 antibody and an antibody directed against an internal and cytoplasmic region of Kkv. Hence, we suggest
574 that the principle mechanism leading to the shed material is the shedding of a vesicle that contains
575 much if not all of Kkv::NG (van Niel et al., 2018).

576 Our in vivo imaging of Kkv::NG provided evidence that Kkv::NG shedding occurs during or after the
577 synthesis of the pupal cuticle. Our ability to detect the shedding was facilitated by the release of the
578 pupal cuticle from the epidermal cells that secrete it. This does not happen with the synthesis of the
579 adult (or larval cuticle) so we were not able to determine if Kkv::NG shedding also happens during the
580 synthesis of the adult cuticle. It is unclear if the shedding is directly related to chitin synthase function
581 (e.g. secreted chitosomes) or if it a consequence of a process that is not directly related to chitin
582 deposition. We did not see evidence of shed puncta when Kkv:: R896K::NG was expressed in wing cells
583 but that could simply be due to the protein not being localized to the apical surface and unrelated to it
584 being catalytically inactive. Our finding that mCD8-GFP is also shed suggests shedding is a general
585 property of membrane proteins either during or after pupal cuticle deposition is complete. It is unclear
586 what if any functional significance is connected to the shedding.

587

588 **Kkv is present in the plasma membrane prior to procuticle formation.**

589 Previous studies on the transcriptome of pupal wing cells (Ren et al., 2005; Sobala and Adler, 2016)
590 established that *kkv* RNA was present prior to the start of wing blade procuticle deposition. Part of the
591 reason for this is that hair chitin is deposited earlier than wing blade chitin. However, this cannot
592 explain the presence of *kkv* RNA 10 hrs prior to the start of hair morphogenesis (Ren et al., 2005) nor the
593 presence of Kkv protein in the general apical membrane (i.e. not in the hair) more than 12 hrs prior to
594 procuticle deposition. These observations suggest the possibility that Kkv has an earlier function in
595 cuticle formation that is not due directly to chitin synthesis (e.g. a structural role for the protein) or that
596 the synthesis of unstable chitin could be important prior to the time when it begins to accumulate. Both

597 of these hypotheses suggest it might be possible to detect abnormalities at early stages of cuticle
598 formation in *kkv* mutant cells. It is worth noting that previously we detected several patches of
599 extracellular chitin fibers on the apical surface of 29 hr awp pupal wings (Sobala et al., 2015). This is 11
600 hrs prior to when we first detect chitin in hairs (Adler et al., 2013) and 3 hours prior to the start of hair
601 outgrowth (Wong and Adler, 1993).

602 **Similarities and differences in bristle and tracheal chitin deposition.**

603 Chitin deposition in bristles and the adult cuticle shows both similarities and differences from that
604 described in trachea. In trachea the distribution of chitin changes during development. Starting out as a
605 thick filament that largely fills the lumen it transforms into a thin zig zag shaped filament. The thin
606 filament is eventually lost and during the this period chitin becomes concentrated over the distinctive
607 tracheal taenidial folds (Devine et al., 2005; Ozturk-Colak et al., 2016; Tonning et al., 2005). It is not
608 clear whether there is a complete loss of the chitin fibrils found in the central filament or if there is a
609 reorganization of those fibrils into the taenidial fold chitin. In both tissues the disruption of the actin
610 cytoskeleton results in an abnormal pattern of chitin; however in tracheal development a lack of chitin
611 lead to an abnormal actin cytoskeleton while we did not see that in wing cells that lacked Kkv (8888). In
612 trachea Kkv puncta were seen more frequently over the taenidial folds than in the inter-fold region
613 (Ozturk-Colak et al., 2016) but the patterning was much less distinctive than we have seen in bristles.
614 Some of the differences between these results could be due to the use of UAS-Gal4 to drive the
615 expression of Kkv in trachea as in our hands using this system resulted in a "messier" pattern than was
616 observed using the edited *kkv* gene. This is presumably due to UAS-Gal4 leading to overexpression.

617

618

619 **Methods and Materials**

620 **Fly Stocks and Genetics**

621 Flies were grown on standard fly food. They were routinely raised at 25°C, but in some experiments,
622 they were raised at 21°C to slow development. In other experiments we used a temperature sensitive
623 Gal80 to limit UAS transgene expression (McGuire et al., 2004). In these experiments, the animals were
624 grown at 21 ^{o}C or 18 ^{o}C and then at the desired stage transferred to 29.5^{o}C to inactivate the Gal80 and
625 induce the expression of the UAS transgene. The various RNAi inducing transgenes came either from the
626 VDRC (Dietzl et al., 2007) or TRiP collections (Perkins et al., 2015). The VDRC lines were obtained from
627 the VDRC (http://stockcenter. vdrc.at/control/main). The TRiP lines were obtained from the
628 Bloomington Drosophila Stock Center (http://flystocks.bio.indiana.edu/) (NIH P40OD018537) as were
629 many other lines used in the research (e.g. Gal4 lines, Df stocks, kkv^{1} carrying stock). Flies that carried a
630 $y\ w\ sn^{3}\ f^{36a}$ X chromosome were kindly provided by G. Guild. Other stocks were made by the author in
631 his lab.

632 **Constructs for generating transgenic lines.**

633 **UAS constructs**

634 The UAS constructs were in the pUAST-attb vector (Bischof et al., 2007). There are 3 *kkv* mRNA isoforms
635 that encode two distinct *kkv* proteins (Thurmond et al., 2018). All of our experiments and analyses were
636 done with the A isoform unless stated otherwise. The C protein isoform is identical to the A isoform and
637 both contain 1615 aa. The D isoform also contains 1615 aa but it differs from the other two proteins by
638 14 aa due to its mRNA containing an alternative coding exon. The 14 amino acids are found in the
639 region bounded by aa 1277 and 1322 of the A isoform. A comparison of the sequence of the genomic
640 *kkv* gene and the longest kkv cDNA (RE32455) from the Drosophila genome project revealed two
641 putative single base pair deletions in RE32455. A comparison of conceptual translation with those of
642 other chitin synthases showed that the genomic sequence was correct. The two single base pair
643 deletions were repaired by site directed mutagenesis to correspond to the genomic sequence. The
644 cDNA was amplified and fused to the coding region for Neon Green by Gibson assembly (NEB-E2611).
645 This fusion gene was inserted into pUAST-attb using added Xho1 and Xba1 sites present in pUAST-attb
646 and added to *kkv::NG* during construction using PCR and oligos containing the sites. This plasmid is
647 referred to as *UAS-kkv::NG*. A similar strategy was used for the construct where the Neon Green tag
648 was replaced by the ollas-his$_6$ (OH) tag. The nucleic acid sequences are provided in supplementary files
649 S1 and S2 and the sequences of the tagged Kkv proteins are provided in files S3 and S4. *The UAS-kkv-*
650 *R896K::NG* plasmid used for transgenesis was made by site directed mutagenesis of *UAS-kkv::NG*.
651 Although an R to K substitution is generally considered a conservative substitution R896 is conserved in
652 all chitin synthases and is thought to be at the catalytic site. In addition, the R to K change is found in
653 the amorphic *kkv*^{1} mutation in Drosophila (Moussian et al., 2005). The same R to K mutation in yeast
654 Chs2 resulted in a reduction to ~ 1% of normal Chs2 enzyme activity (Nagahashi et al., 1995).

655 **The HDR repair constructs**

656 The upstream, middle and downstream repair regions were synthesized by assembly of oligonucleotides
657 by EpochLifeSciences. The segments that comprised Neon Green and smGFP-HA were obtained by PCR
658 from plasmids obtained from Allelebiotech and Addgene (#63166) respectively, added in the correct
659 position by Gibson Assembly. The synthesized segment included several silent mutations to prevent re-
660 cutting by Crispr/Cas9. The repair segments were subcloned into pHD-DsRed vector (Addgene plasmid
661 #51434). The sequences of the plasmids that contain the HDR repair constructs are provided in files S5
662 and S6. The sequences of the Kkv proteins encoded by the two edited genes are provided in File S7 and
663 S8. The construction of the edited genes resulted in a two amino acid linker (AG) between the C
664 terminal aa of kkv and the first amino acid of NG (or smFP). A carton showing the strategy is provided in
665 Fig 1.

666 **gRNA constructs:** Two plasmids that express the needed gRNAs were made by inserting
667 oligonucleotides (files S9) into the pCFD3-cU6:gRNA plasmid where they would be expressed from the
668 pU6-3 promoter (Addgene plasmid #45946).

669 **Transgenic Lines:** Injections of DNA into embryos were done by Rainbow Transgenics. The UAS
670 transgenes were injected into embryos that contained the VK00033 attp landing site (cytol location

671 65B2; 3L:6,442,676..6,442,676). The transgenes were marked by a w^+ gene and Go flies were crossed
672 to w^{1118}; TM3/TM2 flies and the progeny screened for eye color. G1 male flies with eye color were
673 crossed to w; TM3/TM6 female flies and stocks were established by crossing siblings.

674 The HDR construct and the gRNA constructs were both injected into *nos-Cas9* expressing embryos
675 (injections by RainbowTransgenics). The Go flies were crossed to w; TM3/TM2 flies and the G1 flies
676 were screened for candidate edits by the expression of DsRed. Numerous putative edits were obtained
677 by screening for RFP expression from the PhD-Ds-red vector used for HDR. Putative edit containing flies
678 were crossed to w; TM2/TM3 flies and stocks established by crossing siblings that contained the TM3
679 balancer. The Ds-Red expression was monitored and proved to be useful in later stock constructions.
680 We also generated fly stocks where the DsRed was removed by crossing edited male flies to *hs-cre;*
681 *TM3/TM2* females and then crossing *hs-cre; kkv::NG + DS-Red/TM3* males to *w; TM3/TM2* females. The
682 progeny from this cross were screened for *TM3* (and non-*TM2*) flies that did not express Ds-Red. Stocks
683 were established from such single male flies and characterized by PCR to insure they carried the edited
684 Kkv-NG gene but lacked Ds-red sequences. No phenotypic differences were observed between edited
685 flies that carried or did not carry Ds-Red. The presence of Ds-Red expression was convenient for
686 following the edited gene in crosses and it was used for some experiments where we were not imaging
687 an alternative red fluorescent protein or stain.

688 **Characterization of *kkv* edits.** Six independent lines were established for both types of edits. DNA was
689 isolated from these and assayed for the correct DNA changes by PCR followed by sequencing (the oligos
690 used for these experiments are in Table S1). Most of the lines appeared to be as designed and resulted
691 in the in frame fusion of the C terminus of Kkv and the fluorescent protein with the designed two amino
692 acid linker. Three *kkv-NG* and two *kkv-smGFP-HA* lines were retained and further characterized. No
693 differences were seen between the 3 NG edits and between the 2 smGFP edits. One line of each was
694 chosen as the standard for routine use.

695 **Confocal Microscopy**

696 Immunostaining of fixed pupal epidermal cells during the deposition of cuticle is complicated by the
697 inability of the antibodies to penetrate cuticle after the early stages of its development. Thus, most of
698 the imaging experiments we carried out on Kkv in pupae were done by in vivo imaging of Kkv::NG. In a
699 small number of experiments we examined Kkv-NG in fixed tissue. In some we simply used the inherent
700 fluorescence of the neon green tag (sometimes combined with phalloidin staining of actin). In others we
701 used anti-NG immunostaining. Such tissue was only weakly fixed and we did not use animals that were
702 older than around 48 hr after white prepupae (awp). Otherwise, immunostaining of pupal and larval
703 tissues were done as described previously (Nagaraj and Adler, 2012). Imaging of live Kkv::NG containing
704 pupae was done on a Zeiss 780 confocal microscope in the Keck Center for Cellular Imaging. Stained
705 samples were examined on the same microscope.

706

707 **Comparison of *kkv::NG* and *kkv::smFP***

708 We estimated the brightness difference between the products of the *kkv::NG* and *kkv::smFP* edited
709 genes by live imaging both in the same confocal session using the same microscope conditions. We
710 measured the brightness of maximal projections of both types of animals and then subtracted the
711 background brightness. The ratio of brightness for *kkv::NG* and *kkv::smFP* was 14.7. To estimate the
712 relative amount of the two proteins present we needed to correct for the relative brightness of the two
713 fluorescent protein tags. We were unable to find a value for the brightness of *smFP* but we were able to
714 find a value for the progenitor of smFP, superfolder GFP and Neon-Green (Lambert and Thorn, 2019).
715 The relative brightness was 1.7, which gave an estimate that Kkv::NG was present in 8.65 fold higher
716 concentration than Kkv::smFP. Assuming Kkv::smFP has the same specific activity as wild type Kkv we
717 estimate the *kkv::smFP* cells only contain about 11% of the normal Kkv enzyme activity.

718

719 **Kkv topology experiments**

720 We obtained predictions for the number and locations of transmembrane domains from the following
721 programs: TMHMM2.0, TMPRED, Uniprot, PHDhtm and CCTOP. The CCTOP site returned predictions for
722 HMMTOP, Memsat, Octopus, Philius, Phobius, Pro, Prodiv, Scampi, ScampiMsa as well as CCTOP. 14
723 putative transmembrane domains were predicted by 13 or 14 of these 14 programs. These "consensus
724 sites are shown in Fig 6 and the specific TMHMM2.0 predictions are provided in Table S2. The specific
725 amino acids predicted to be in each transmembrane domain were often shifted by a few amino acids by
726 different programs but the putative transmembrane domains substantially overlapped.

727 To examine the topology of Kkv we drove the expression of *UAS-kkv-OH* or *UAS-kkv::NG* by *ptc-GAL4*.
728 This results in a stripe of expression along the anterior/posterior compartment boundary in wing discs.
729 Wing discs were dissected in PBS and fixed in the cold for 15'. The discs were then manually cut or
730 punctured to ensure the apical surface of the epithelial cells was exposed to antibody. They were then
731 incubated for 30' in PBS supplemented with 10% Sheep Serum. The discs were then stained overnight at
732 4°C in PBS, 10% sheep serum plus the desired antibody. The discs were then rinsed 4 times in PBS and
733 then stained with secondary antibody for 3 hrs at room temperature in PBS, 10% sheep serum plus
734 secondary antibody. After 4 rinses in PBS the discs were washed with PBST (PBS plus .3% triton X100)
735 followed by three additional washes in PBS. Finally the discs were mounted in ProLong Diamond. As a
736 control several of the fixed and cut discs had PBST substituted for PBS in all steps in the experiment. The
737 wing discs were examined on a Zeiss Axioskop II and photographed on a Spot Digital Camera (National
738 Diagnostics).

739

740 **Scanning Electron Microscopy**

741 Wings were removed from two day old adult flies. In the experiments described in the paper the wings
742 contained flip out clones (AyGal4) that expressed an RNAi for *kkv* (Trip line – HMC.05880). The hair
743 phenotype overlapped with that seen previously in clones homozygous for kkv^{1} with but with a smaller
744 fraction with the strongest phenotype (Ren et al., 2005). The wings were attached to studs with a

745 vertical surface with conducting paint and they were then fractured with a tungsten needle. They were
746 shadowed with platinum and examined in a Zeiss Sigma VP HD field emission Scanning Electron
747 Microscpe (SEM) (NIH 1S10OD011966-01A1) at the University of Virginia Advanced Microscopy Facility.

748

749 **Figure Legends**

750 Figure 1. A. Models for the the relationship between Chitin Synthase and the patterned deposition of
751 chitin. B. Cartoons showing the proteins encoded by both UAS transgenes and edited genes. The
752 asterisks indicates the R896K mutation. C. The approach used for the editing of *kkv*. The upward
753 arrows indicate the target locations of the two guide RNAs. The upper part of the panel shows the 3'
754 end of *kkv.*

755 Figure 2. The rescue of the wing phenotype of *kkv::smFP* by the expression of a UAS transgene driven by
756 *ap-Gal4.* A small region from the dorsal and ventral surface of the wing is shown for all genotypes. This
757 region is from the posterior region. Note the thin bent hairs on both surfaces of the *kkv::smFP*
758 homozygotes (EF) compared to those in wild type (AB) and *ap>kkv::NG* (CD) wings. Note the rescue in
759 the dorsal surface of *ap>kkv::NG; kkv::smFP/Df* wings (GH). This is due to *ap* only driving expression of
760 UAS transgenes in the dorsal surface cells. Note the failure to see rescue in *ap>kkv R896K::NG;*
761 *kkv::smFP* wings (IJ) establishing that only the expression of a functional Kkv protein provides rescue.

762 Figure 3. Localization of Kkv. A. A low magnification image of a *kkv::NG* notum. B. A higher
763 magnification image of part of a *kkv::NG* notum. Note the stripes of Kkv::NG along the proximal distal
764 axis of the bristles. The arrows point to several of the fluorescent puncta associated with the expression
765 of *kkv::NG.* C (C' and C''). A high magnification image of a bristle from a *UAS-ChtVis/+; neur-Gal4/*
766 *kkv::NG/+* bristle. Note the relatively smooth bands of chitin and the punctate stripes of Kkv::NG and
767 the association between the two. D,E,F. Two bristles from a *neur-Gal4/kkv::NG* pupae immunostained
768 for NeonGreen (green-D) and Kkv (red-F). E is the merged image and shows the high degree of co-
769 immunostaining. G,H,I. Bristles from a *neur-Gal4/kkv-OH* pupae immunostained for ollas (green-G) and
770 Kkv (red-I). H is the merged image and shows the high degree of co-immunostaining. J,K,L. A bristle
771 from a *neur-Gal4/UAS-kkv R896K::NG* pupae immunostained for NeonGreen (green-J) and Kkv (red-L). K
772 is the merged image and shows the high degree of co-immunostaining. Note the pattern of
773 accumulation of Kkv R896K::NG is quite abnormal and shows substantial bristle to bristle variation but
774 the co-localization is consistent. M,N,O. Pupal wings from *ap-Gal4/+; UAS-kkv::NG* immuostained for
775 NeonGreen (green-M) and Kkv (red-P). N is the mergred imaged and shows the high degree of co-
776 localization. P,Q,R. Pupal wings from *ap-Gal4/+; UAS-kkv R896K::NG* immuostained for NeonGreen
777 (green-M) and Kkv (red-P). N is the mergred imaged and shows the localization of the mutant protein is
778 highly abnormal but the high degree of co-localization remains.

779 Figure 4. Localization of Kkv in the pupal wing. A-F. In vivo images of *kkv::NG* pupal wings. All except B
780 are shown with the same microscope settings. Note the clear labeling of the hairs in wings from 42-58
781 hr. In the oldest wings the hairs are fainter and the image is from the focal plane where the pedestals
782 are obvious. We did not detect hair labeling in the youngest wings (A) unless the image was enhance by

783 brightening in ImageJ or Photoshop (B). G,H,I. Shown is a *ap-Gal4/+; UAS-kkv::NG* pupal 36 hr wing
784 fixed and F-actin stained with phalloidin (red). Note the NeonGreen is external to the F-actin. One can
785 also see that the NeonGreen signal is in the hair membrane and does not extend to the center of the
786 hair. J,K,L. A fixed 48 hr *ap-Gal4/+; UAS-kkv::NG* wing stained for both NeonGreen (J-green) and F-actin
787 (L-phalloidin - red). Note the bright disc of F-actin staining at the base of the hair is not associated with
788 an accumulation of Kkv::NG.

789 Figure 5. Factors that mediate the localization of Kkv in stripes in bristles. A. A *sn f; kkv::NG* bristle by in
790 vivo imaging. The lack of the large F-actin bundles due to the loss of *sn* and *f* leads to highly abnormal
791 shape and abnormal pattering of Kkv::NG stripes. B. A *sn f;UAS-ChtVis/+; neur-Gal4/+* bristle by in vivo
792 imaging. The lack of the large F-actin bundles due to the loss of *sn* and *f* leads to highly abnormal bristle
793 shape and to abnormal patterning of chitin. C,D,E. A *sn f; UAS-ChtVis/+; neur-Gal4 kkv::NG/kkv::NG*
794 bristle by in vivo imaging. The lack of the large F-actin bundles due to the loss of *sn* and *f* leads to highly
795 abnormal shape and abnormal patterning of both chitin (C - red) and Kkv::NG (E – green) stripes. Note
796 the close association of Kkv and chitin (D- merged image, arrow) even though the pattern as a whole is
797 highly abnormal. F. A *UAS-dyl RNAi; neur-Gal4 kkv::NG/kkv::NG* thorax by in vivo imaging. Note the
798 bulged bristle (arrow) and the lack/great reduction of Kkv stripes. G A *UAS-Rab11-RNAi; neur-Gal4*
799 *kkv::NG/kkv::NG* bristle by in vivo imaging. Note the stub bristle phenotype (arrow) and the lack of
800 Kkv::NG stripes. H,I,J. A UAS-Ruby-Lifeact; *neur-Gal4 kkv::NG/kkv::NG* bristle showing the large bundles
801 of F-actin (H – red) and stripes of Kkv::NG (J – green). H', I',L' are higher magnification images where the
802 overlap between the F-actin bundles and Kkv::NG stripes is obvious. KLM. *Kkv::NG* bristles
803 immunostained with anti-Dyl antibody (K – red) and anti-NeonGreen antibody (M – green). In the
804 merged image (L) the interdigitated stripes of red and green can be seen (arrow). N-S. Orthogonal
805 cross sections of bristles of various genotypes. N. *kkv::NG* shows a distinct pattern of stripes. O. *UAS-*
806 *ChtVis/+; neur-Gal4 kkv::NG/kkv::NG* shows the close association of the chitin bands and the stripes of
807 Kkv::NG. In many cases the chitin is external to Kkv::NG (arrows). P. *UAS-Rab11-RNAi; neur-Gal4*
808 *kkv::NG/kkv::NG* bristles show a failure in the localization of Kkv to the plasma membrane. Q. *UAS-dyl*
809 *RNAi; neur-Gal4 kkv::NG/kkv::NG* bristles show much of the Kkv::NG is inserted into the plasma
810 membrane but it is not localized into the strip pattern (e.g. N). R. *sn f; kkv::NG* bristles have an
811 abnormal cross section and evidence for abnormal stripes of Kkv::NG are evident (arrows). S. *sn f; UAS-*
812 *ChtVis; neur-Gal4 kkv::NG/kkv::NG* bristles show the expected abnormal cross section shape with the
813 irregular banding of Kkv::NG and chitin. Note the close association of Kkv::NG and chitin (arrows) even
814 in these very abnormal bristles.

815 Fig 6. Topology of Kkv. A. *ptc-Gal4 UAS-kkv::NG* (or *UAS-kkv*-OH) wing discs where *kkv* is expressed in a
816 stripe immunostained with various antibodies with or without detergent treatment (PBS vs PBST). B. A
817 cartoon showing the consensus transmembrane domains as described in the Methods. The location of
818 the epitope recognized by each of the antibodies. The data indicate that the amino terminus is
819 cytoplasmic and the carboxy terminus is extracellular.

820 Fig 7. Expression of *kkv::NG* leads to fluorescent puncta in the space between the pupal cuticle and the
821 apical surface of the notum epithelial cells. A, B, C. *kkv::NG* pupae. D, E, F. Oregon R pupae. G, H, I.
822 *ap-Ga4; UAS-mCD8*-GFP. A, D and G are maximal projections of the optical stack regions that encompass

823 the notum pupal cuticle. The arrow in A and G points to a likely puncta and the arrowheads to the
824 patterned brightness seen in the pupal cuticle of animals that express a fluorescent membrane protein.
825 B, E and H are maximal projections of the optical stack regions that encompass the region between the
826 notum pupal cuticle and the upper most region of the notum epithelial cells (i.e. the bristles that extend
827 apically). Since there was no fluorescence in E we took the conservative approach of extending this
828 region of the stack by 50%. The arrows in B and H point to one of the many fluorescent puncta. C, F and
829 I are maximal projections of the optical stack regions that encompass the region of cellular material
830 including bristles, hairs and the apical surface of the notum cells. The arrows points to fluorescent
831 puncta.

832 Fig 8. Examination of *kkv* mutant clones by SEM. A. Three possible models for the phenotypic effects of
833 a *kkv* mutant cell (in green) on it and its neighbors. In the uppermost the mutant phenotype is rescued
834 by neighboring wild type cells. In the middle panel the inability to synthesize chitin results in a thinner
835 wing cuticle and this is hypothesized to be entirely cell autonomous. In the lowest most panel there is
836 partial rescue of the ability to synthesize chitin and this is graded from neighboring to mutant cell. B. A
837 relatively low magnification SEM image of a fractured adult wing that contains a clone of *kkv* mutant
838 cells. Arrows point to two of these. C. A region of a wing without any *kkv* clones. Note the relatively
839 consistent cuticle thickness and the parallel layers. D. A region of a wing that contains a mutant cell
840 (mutant hair marked by an arrow). Note how thin the mutant cuticle is (arrowhead) compared to the
841 neighboring wild type cuticle (asterisk). Note also that there is a smooth and graded transition between
842 the mutant and neighboring cell cuticle. E. Another example of a *kkv* mutant clone as in D.

843

844 Supplemental Figure Legends.

845 Fig S1. The melanotic spot phenotype. A. No melanotic spot phenotype is seen in hypomorphic
846 *kkv::smFP/Df* flies. B. The over expression of the catalytically inactive Kkv R896K mutant driven by *ap-*
847 *Gal4* results in the melanotic spot (arrow) phenotype. C. The over expression of Kkv::NG driven by *ap-*
848 *Gal4* results in the melanotic spot (arrow) phenotype.

849 Fig S2. SEM examination of wing cuticle of edited flies. A. Flies homozygous for *kkv::smFP* show the thin
850 bent and curved wing hair phenotype. B. *kkv::smFP/Df* flies show a slightly enhanced wing hair
851 phenotype. C. Flies homozygous for *kkv::NG* have normal wing hairs. D. *Kkv::NG/DF* flies also have normal
852 wing hairs. E. Oregon R wild type flies have normal wing hairs. F. Ore-R/Df flies also have normal wing
853 hairs showing that *kkv* is not haplo-insufficient.

854 Fig S3. *kkv::NG* is much brighter than *kkv::smFP.* A. Image of live *kkv::NG* thorax (maximal projection) as
855 obtained from the confocal with no modifications. The arrows point to fluorescent puncta. The image
856 was obtained with a lower laser power than we typically used to increase the range of brightness. B image
857 of live *kkv::smFP* as obtained from the confocal using the same settings as in A. C. The image from A
858 brightened in Photoshop by +150. D. The image in B brightened in Photoshop by +150. E. The image in C
859 brightened by a further +150. F. The image from D brightened by a further +150. G. The image from E
860 with both the brightness and contrast increased by 150. H. The image from E with both the brightness

861 and contrast increased by 150. Hairs on the notum are finally visible and a bristle is barely visible. The
862 asterisks mark pupal cuticle. The *kkv::NG* animal was a few hrs younger (48 hr awp) than the *kkv::smFP*
863 animal (52 hr awp). Since 52 hr animals show slightly higher fluorescence this figure slightly
864 underestimates the difference in brightness.

865 Fig S4. Comparison of the subcellular localization of Kkv::NG and Kkv R896K::NG. A. Image of live 44hr
866 ap>*kkv::NG* pupal wing. B. Image of live 44hr ap>*kkv-R896K::NG* pupal wing. C. Image of a 36hr
867 ap>*kkv::NG* pupal wing fixed and stained with both anti-NG antibody (green) and Alexa 568 phalloidin
868 (red) to shoe F-actin. D. Image of a 36hr ap>*kkv R896K::NG* pupal wing fixed and stained with both anti-
869 NG antibody (green) and Alexa 568 phalloidin (red) to shoe F-actin. E. Image of a live 52 hr ap>*kkv::NG*
870 pupal wing showing a bristle with Kkv stripes. The arrows point to shed fluorescent puncta. F. Image of a
871 live 52 hr ap>*kkv R896K::NG* pupal wing showing a bristle with abnormal accumulation of Kkv. G.
872 Orthogonal cross sections of bristles from *ap>kkv::NG* live pupae. H. Orthogonal cross sections of bristles
873 from *ap>kkv R896K::NG* live pupae. Note the stripes in G and the mislocalized Kkv in H. I. A live dissected
874 salivary gland from a *ptc-Gal4/+; UAS-kkv::NG* third instar larva. The Kkv::NG preferentially accumulates
875 on the apical surface of the gland (arrow) next to the lumen (asterisk). I' is a blow up of a single optical
876 section of a *ptc-Gal4/+; UAS-kkv::NG* salivary gland. Note the many round vesicles with puncta obvious in
877 the membrane of these vesicles (arrow). J. A live dissected salivary gland from a *ptc-Gal4/+; UAS-kkv*
878 *R896K::NG* third instar larva. The Kkv R896K::NG does not preferentially accumulate on the apical surface
879 of the gland next to the lumen (asterisk). Rather, it is rather evenly distributed across the cytoplasm. J'.
880 The blow up shows a different morphology in how the protein accumulates compared to Kkv::NG (I').

881 Fig S5. Specificity of Kkv staining. A. A *ptc-Gal4/UAS-ChtVis; UAS-kkv::NG* wing disc shows the
882 accumulation of Kkv::NG in the *ptc* domain (arrow). The secreted ChtVis (red) diffuses all over the disc
883 in the extracellular domin that separates the disc epithelium and the peripodial membrane. B. Kkv::NG
884 preferentially accumulates on the apical surface of disc cells (arrow). C-F. Comparisons of *kkv::NG* (CE)
885 and Ore-R (DF) 63 hr awp pupae by live imaging. C and D were taken at the same microscope settings as
886 were E and F. Note the bristle, hair and cell membrane fluorescence of Kkv::NG is specific and not seen
887 in Ore-R. The arrows in C and D point to auto-flourescent pupal cuticle. E and F are higher
888 magnification images that show the stripes of Kkv::NG in bristles and the lack of such fluorescence in
889 Ore-R.
890
891 Fig S6. Kkv::NG fluorescence as a function of developmental time since white prepuae formation. All
892 images were taken at the same microscope setting.
893
894 Fig S7. How geometry affects optical sectioning of bristles. A cartoon of a bristle (B) in cross section is
895 shown with intracellular bands of red and extracellular bands of green. The arrows indicate different
896 planes of sectioning and the images the arrow point to show the expected resulting images and how
897 these can differ depending on the location and orientation of the optical sections.
898
899 Fig S8. The accumulation of Dyl in stripes in bristles is altered in sn f double mutants. A. A *sn f* bristle
900 immunostained with anti-Dyl antibodies. Note the parallel lines of Dyl staining (Nagaraj and Adler,

2012) are disrupted. B. Cross sections of several *sn f* bristles immunostained for Dyl. Note the disruption in staining and the retention of lines of Dyl is variable from bristle to bristle.

Fig S9. Kkv::NG dependent puncta in live pupae. A. Many puncta (arrow) are visible in the space between the pupal cuticle and the notum epidermis in 50 hr awp pupa. The pupal cuticle is visible (asterisk) due to autoflourescence. B. Puncta are visible and concentrated along the mid line of a 20 hr awp *kkv::NG* pupa. At this time the epidermal cells are still attached to the pupal cuticle they synthesized so the cellular outlines are visible. C. Puncta are visible (arrow) in the space between the pupal cuticle and the notum epidermis in 50 hr awp *ap-Gal4/+; UAS-kkv::NG/+* pupa. D. No puncta are visible (arrow) in the space between the pupal cuticle and the notum epidermis in 50 hr awp *ap-Gal4/+; UAS-kkv R896K::NG/+* pupa. This is likely due primarily to the protein not being localized properly to the apical surface.

Fig s10. Puncta associated with pupal cuticle can be stained with both anti-NG and anti-Kkv antibodies. Pupal cuticle was fixed and dissected from 42 hr *kkv::NG* pupae and immunostained with both anti-NG and anti-Kkv antibodies. Many puncta were visible and a large number of these stained with both antibodies consistent with the hypothesis that the puncta visualized by in vivo imaging of NeonGreen also contained Kkv.

Acknowledgements

This research was supported by funds provided by the W. R. Kenan Chair to the author and to a limited extent personal funds of the author. The author thanks H.S. Tzu for helpful conversations. "We acquired confocal images using the Keck Center Zeiss 780 Confocal microscopy system (NIH OD016446). We acquired Scanning Electron Microscope images at the Advanced Microscopy Facility at the University of Virginia. The images were obtained on a Zeiss VP HD SEM field purchased with a grant from the NIH (NIH 1S10OD011966).

References

Adler, P. N. (2017). Gene expression and morphogenesis during the deposition of Drosophila wing cuticle. *Fly (Austin)* **11**, 194-199.

Adler, P. N., Sobala, L. F., Thom, D. and Nagaraj, R. (2013). dusky-like is required to maintain the integrity and planar cell polarity of hairs during the development of the Drosophila wing. *Developmental biology* **379**, 76-91.

Bischof, J., Maeda, R. K., Hediger, M., Karch, F. and Basler, K. (2007). An optimized transgenesis system for Drosophila using germ-line-specific phiC31 integrases. *Proceedings of the National Academy of Sciences of the United States of America* **104**, 3312-3317.

939 **Bouligand, Y.** (1972). Twisted fibrous arrangements in biological materials and cholesteric mesophases.
940 *Tissue Cell* **4**, 189-217.
941 **Broehan, G., Zimoch, L., Wessels, A., Ertas, B. and Merzendorfer, H.** (2007). A chymotrypsin-like serine
942 protease interacts with the chitin synthase from the midgut of the tobacco hornworm. *J Exp Biol*
943 **210**, 3636-3643.
944 **Cabib, E. and Bowers, B.** (1971). Chitin and yeast budding. Localization of chitin in yeast bud scars. *J Biol*
945 *Chem* **246**, 152-159.
946 **Calero-Cuenca, F. J. and Sotillos, S.** (2018). Nuf and Rip11 requirement for polarity determinant
947 recycling during Drosophila development. *Small GTPases* **9**, 352-359.
948 **Chanut-Delalande, H., Ferrer, P., Payre, F. and Plaza, S.** (2012). Effectors of tridimensional cell
949 morphogenesis and their evolution. *Seminars in cell & developmental biology* **23**, 341-349.
950 **Chaudhari, S. S., Arakane, Y., Specht, C. A., Moussian, B., Boyle, D. L., Park, Y., Kramer, K. J., Beeman,**
951 **R. W. and Muthukrishnan, S.** (2011). Knickkopf protein protects and organizes chitin in the
952 newly synthesized insect exoskeleton. *Proceedings of the National Academy of Sciences of the*
953 *United States of America* **108**, 17028-17033.
954 **Chuang, J. S. and Schekman, R. W.** (1996). Differential trafficking and timed localization of two chitin
955 synthase proteins, Chs2p and Chs3p. *J Cell Biol* **135**, 597-610.
956 **Devine, W. P., Lubarsky, B., Shaw, K., Luschnig, S., Messina, L. and Krasnow, M. A.** (2005). Requirement
957 for chitin biosynthesis in epithelial tube morphogenesis. *Proceedings of the National Academy of*
958 *Sciences of the United States of America* **102**, 17014-17019.
959 **Dietzl, G., Chen, D., Schnorrer, F., Su, K. C., Barinova, Y., Fellner, M., Gasser, B., Kinsey, K., Oppel, S.,**
960 **Scheiblauer, S., et al.** (2007). A genome-wide transgenic RNAi library for conditional gene
961 inactivation in Drosophila. *Nature* **448**, 151-156.
962 **Dorfmueller, H. C., Ferenbach, A. T., Borodkin, V. S. and van Aalten, D. M.** (2014). A structural and
963 biochemical model of processive chitin synthesis. *J Biol Chem* **289**, 23020-23028.
964 **Dos Santos, G., Schroeder, A. J., Goodman, J. L., Strelets, V. B., Crosby, M. A., Thurmond, J., Emmert,**
965 **D. B., Gelbart, W. M. and FlyBase, C.** (2015). FlyBase: introduction of the Drosophila
966 melanogaster Release 6 reference genome assembly and large-scale migration of genome
967 annotations. *Nucleic acids research* **43**, D690-697.
968 **Elieh-Ali-Komi, D. and Hamblin, M. R.** (2016). Chitin and Chitosan: Production and Application of
969 Versatile Biomedical Nanomaterials. *Int J Adv Res (Indore)* **4**, 411-427.
970 **Fernandes, I., Chanut-Delalande, H., Ferrer, P., Latapie, Y., Waltzer, L., Affolter, M., Payre, F. and Plaza,**
971 **S.** (2010). Zona pellucida domain proteins remodel the apical compartment for localized cell
972 shape changes. *Dev Cell* **18**, 64-76.
973 **Foltman, M., Filali-Mouncef, Y., Crespo, D. and Sanchez-Diaz, A.** (2018). Cell polarity protein Spa2
974 coordinates Chs2 incorporation at the division site in budding yeast. *PLoS genetics* **14**,
975 e1007299.
976 **Gohlke, S., Muthukrishnan, S. and Merzendorfer, H.** (2017). In Vitro and In Vivo Studies on the
977 Structural Organization of Chs3 from Saccharomyces cerevisiae. *Int J Mol Sci* **18**.
978 **Guild, G. M., Connelly, P. S., Vranich, K. A., Shaw, M. K. and Tilney, L. G.** (2002). Actin filament turnover
979 removes bundles from Drosophila bristle cells. *Journal of cell science* **115**, 641-653.
980 **Hatan, M., Shinder, V., Israeli, D., Schnorrer, F. and Volk, T.** (2011). The Drosophila blood brain barrier
981 is maintained by GPCR-dependent dynamic actin structures. *J Cell Biol* **192**, 307-319.
982 **Hernandez-Gonzalez, M., Bravo-Plaza, I., Pinar, M., de Los Rios, V., Arst, H. N., Jr. and Penalva, M. A.**
983 (2018). Endocytic recycling via the TGN underlies the polarized hyphal mode of life. *PLoS*
984 *genetics* **14**, e1007291.
985 **Jovine, L., Darie, C. C., Litscher, E. S. and Wassarman, P. M.** (2005). Zona pellucida domain proteins.
986 *Annual review of biochemistry* **74**, 83-114.

Jovine, L., Qi, H., Williams, Z., Litscher, E. and Wassarman, P. M. (2002). The ZP domain is a conserved module for polymerization of extracellular proteins. *Nature cell biology* **4**, 457-461.

Karouzou, M. V., Spyropoulos, Y., Iconomidou, V. A., Cornman, R. S., Hamodrakas, S. J. and Willis, J. H. (2007). Drosophila cuticular proteins with the R&R Consensus: annotation and classification with a new tool for discriminating RR-1 and RR-2 sequences. *Insect biochemistry and molecular biology* **37**, 754-760.

Knafler, H. C., Smaczynska-de, R., II, Walker, L. A., Lee, K. K., Gow, N. A. R. and Ayscough, K. R. (2019). AP-2-Dependent Endocytic Recycling of the Chitin Synthase Chs3 Regulates Polarized Growth in Candida albicans. *MBio* **10**.

Kozubowski, L., Panek, H., Rosenthal, A., Bloecher, A., DeMarini, D. J. and Tatchell, K. (2003). A Bni4-Glc7 phosphatase complex that recruits chitin synthase to the site of bud emergence. *Mol Biol Cell* **14**, 26-39.

Lambert, T. and Thorn, K. (2019). FPbase.org - The Fluorescent Protein Database.

Latge, J. P., Mouyna, I., Tekaia, F., Beauvais, A., Debeaupuis, J. P. and Nierman, W. (2005). Specific molecular features in the organization and biosynthesis of the cell wall of Aspergillus fumigatus. *Med Mycol* **43 Suppl 1**, S15-22.

Leal-Morales, C. A., Bracker, C. E. and Bartnicki-Garcia, S. (1994). Subcellular localization, abundance and stability of chitin synthetases 1 and 2 from Saccharomyces cerevisiae. *Microbiology* **140 (Pt 9)**, 2207-2216.

Lichtenthaler, S. F., Lemberg, M. K. and Fluhrer, R. (2018). Proteolytic ectodomain shedding of membrane proteins in mammals-hardware, concepts, and recent developments. *EMBO J* **37**.

Maue, L., Meissner, D. and Merzendorfer, H. (2009). Purification of an active, oligomeric chitin synthase complex from the midgut of the tobacco hornworm. *Insect biochemistry and molecular biology* **39**, 654-659.

McGuire, S. E., Mao, Z. and Davis, R. L. (2004). Spatiotemporal gene expression targeting with the TARGET and gene-switch systems in Drosophila. *Sci STKE* **2004**, pl6.

Merzendorfer, H. (2006). Insect chitin synthases: a review. *J Comp Physiol B* **176**, 1-15.

The cellular basis of chitin synthesis in fungi and insects: common principles and differences. *European journal of cell biology* **90**, 759-769.

Merzendorfer, H. and Zimoch, L. (2003). Chitin metabolism in insects: structure, function and regulation of chitin synthases and chitinases. *J Exp Biol* **206**, 4393-4412.

Moussian, B. (2013). The apical plasma membrane of chitin-synthesizing epithelia. *Insect science* **20**, 139-146.

Moussian, B., Letizia, A., Martinez-Corrales, G., Rotstein, B., Casali, A. and Llimargas, M. (2015). Deciphering the genetic programme triggering timely and spatially-regulated chitin deposition. *PLoS genetics* **11**, e1004939.

Moussian, B., Schwarz, H., Bartoszewski, S. and Nusslein-Volhard, C. (2005). Involvement of chitin in exoskeleton morphogenesis in Drosophila melanogaster. *Journal of morphology* **264**, 117-130.

Moussian, B., Seifarth, C., Muller, U., Berger, J. and Schwarz, H. (2006a). Cuticle differentiation during Drosophila embryogenesis. *Arthropod structure & development* **35**, 137-152.

Moussian, B., Tang, E., Tonning, A., Helms, S., Schwarz, H., Nusslein-Volhard, C. and Uv, A. E. (2006b). Drosophila Knickkopf and Retroactive are needed for epithelial tube growth and cuticle differentiation through their specific requirement for chitin filament organization. *Development* **133**, 163-171.

Moussian, B., Veerkamp, J., Muller, U. and Schwarz, H. (2007). Assembly of the Drosophila larval exoskeleton requires controlled secretion and shaping of the apical plasma membrane. *Matrix biology : journal of the International Society for Matrix Biology* **26**, 337-347.

1034 **Muszkieta, L., Aimanianda, V., Mellado, E., Gribaldo, S., Alcazar-Fuoli, L., Szewczyk, E., Prevost, M. C.**
1035 **and Latge, J. P.** (2014). Deciphering the role of the chitin synthase families 1 and 2 in the in vivo
1036 and in vitro growth of Aspergillus fumigatus by multiple gene targeting deletion. *Cell Microbiol*
1037 **16**, 1784-1805.
1038 **Nagahashi, S., Sudoh, M., Ono, N., Sawada, R., Yamaguchi, E., Uchida, Y., Mio, T., Takagi, M., Arisawa,**
1039 **M. and Yamada-Okabe, H.** (1995). Characterization of chitin synthase 2 of Saccharomyces
1040 cerevisiae. Implication of two highly conserved domains as possible catalytic sites. *J Biol Chem*
1041 **270**, 13961-13967.
1042 **Nagaraj, R. and Adler, P. N.** (2012). Dusky-like functions as a Rab11 effector for the deposition of cuticle
1043 during Drosophila bristle development. *Development* **139**, 906-916.
1044 **Ostrowski, S., Dierick, H. A. and Bejsovec, A.** (2002). Genetic control of cuticle formation during
1045 embryonic development of Drosophila melanogaster. *Genetics* **161**, 171-182.
1046 **Ozturk-Colak, A., Moussian, B., Araujo, S. J. and Casanova, J.** (2016). A feedback mechanism converts
1047 individual cell features into a supracellular ECM structure in Drosophila trachea. *Elife* **5**.
1048 **Park, S. H., Cheong, C., Idoyaga, J., Kim, J. Y., Choi, J. H., Do, Y., Lee, H., Jo, J. H., Oh, Y. S., Im, W., et al.**
1049 (2008). Generation and application of new rat monoclonal antibodies against synthetic FLAG and
1050 OLLAS tags for improved immunodetection. *J Immunol Methods* **331**, 27-38.
1051 **Perkins, L. A., Holderbaum, L., Tao, R., Hu, Y., Sopko, R., McCall, K., Yang-Zhou, D., Flockhart, I., Binari,**
1052 **R., Shim, H. S., et al.** (2015). The Transgenic RNAi Project at Harvard Medical School: Resources
1053 and Validation. *Genetics* **201**, 843-852.
1054 **Polko, J. K. and Kieber, J. J.** (2019). The Regulation of Cellulose Biosynthesis in Plants. *Plant Cell* **31**, 282-
1055 296.
1056 **Ren, N., Zhu, C., Lee, H. and Adler, P. N.** (2005). Gene expression during Drosophila wing morphogenesis
1057 and differentiation. *Genetics* **171**, 625-638.
1058 **Riedl, J., Crevenna, A. H., Kessenbrock, K., Yu, J. H., Neukirchen, D., Bista, M., Bradke, F., Jenne, D.,**
1059 **Holak, T. A., Werb, Z., et al.** (2008). Lifeact: a versatile marker to visualize F-actin. *Nat Methods*
1060 **5**, 605-607.
1061 **Ryder, E., Ashburner, M., Bautista-Llacer, R., Drummond, J., Webster, J., Johnson, G., Morley, T., Chan,**
1062 **Y. S., Blows, F., Coulson, D., et al.** (2007). The DrosDel deletion collection: a Drosophila
1063 genomewide chromosomal deficiency resource. *Genetics* **177**, 615-629.
1064 **Sacristan, C., Manzano-Lopez, J., Reyes, A., Spang, A., Muniz, M. and Roncero, C.** (2013).
1065 Oligomerization of the chitin synthase Chs3 is monitored at the Golgi and affects its endocytic
1066 recycling. *Mol Microbiol* **90**, 252-266.
1067 **Saiz-Baggetto, S., Mendez, E., Quilis, I., Igual, J. C. and Bano, M. C.** (2017). Chimeric proteins tagged
1068 with specific 3xHA cassettes may present instability and functional problems. *PLoS One* **12**,
1069 e0183067.
1070 **Santos, B. and Snyder, M.** (1997). Targeting of chitin synthase 3 to polarized growth sites in yeast
1071 requires Chs5p and Myo2p. *J Cell Biol* **136**, 95-110.
1072 **Shaner, N. C., Lambert, G. G., Chammas, A., Ni, Y., Cranfill, P. J., Baird, M. A., Sell, B. R., Allen, J. R.,**
1073 **Day, R. N., Israelsson, M., et al.** (2013). A bright monomeric green fluorescent protein derived
1074 from Branchiostoma lanceolatum. *Nat Methods* **10**, 407-409.
1075 **Sobala, L. F. and Adler, P. N.** (2016). The Gene Expression Program for the Formation of Wing Cuticle in
1076 Drosophila. *PLoS genetics* **12**, e1006100.
1077 **Sobala, L. F., Wang, Y. and Adler, P. N.** (2015). ChtVis-Tomato, a genetic reporter for in vivo visualization
1078 of chitin deposition in Drosophila. *Development* **142**, in press.
1079 **Thurmond, J., Goodman, J. L., Strelets, V. B., Attrill, H., Gramates, L S., Marygold, S. J., Matthews, B.**
1080 **B., Millburn, G., Antonazzo, G., Trovisco, V., et al.** (2018). FlyBase 2.0: the next generation.
1081 *Nucleic acids research* **47**, D759-D765.

1082 **Tilney, L. G., Connelly, P. S., Ruggiero, L., Vranich, K. A., Guild, G. M. and Derosier, D.** (2004). The role
1083 actin filaments play in providing the characteristic curved form of Drosophila bristles. *Mol Biol*
1084 *Cell* **15**, 5481-5491.
1085 **Tilney, L. G., Tilney, M. S. and Guild, G. M.** (1995). F actin bundles in Drosophila bristles. I. Two filament
1086 cross-links are involved in bundling. *J Cell Biol* **130**, 629-638.
1087 **Tonning, A., Hemphala, J., Tang, E., Nannmark, U., Samakovlis, C. and Uv, A.** (2005). A transient luminal
1088 chitinous matrix is required to model epithelial tube diameter in the Drosophila trachea. *Dev*
1089 *Cell* **9**, 423-430.
1090 **Turner, C. M. and Adler, P. N.** (1998). Distinct roles for the actin and microtubule cytoskeletons in the
1091 morphogenesis of epidermal hairs during wing development in Drosophila. *Mech Dev* **70**, 181-
1092 192.
1093 **van Niel, G., D'Angelo, G. and Raposo, G.** (2018). Shedding light on the cell biology of extracellular
1094 vesicles. *Nat Rev Mol Cell Biol* **19**, 213-228.
1095 **Viswanathan, S., Williams, M. E., Bloss, E. B., Stasevich, T. J., Speer, C. M., Nern, A., Pfeiffer, B. D.,**
1096 **Hooks, B. M., Li, W. P., English, B. P., et al.** (2015). High-performance probes for light and
1097 electron microscopy. *Nat Methods* **12**, 568-576.
1098 **Welz, T., Wellbourne-Wood, J. and Kerkhoff, E.** (2014). Orchestration of cell surface proteins by Rab11.
1099 *Trends Cell Biol* **24**, 407-415.
1100 **Willis, J. H.** (2010). Structural cuticular proteins from arthropods: annotation, nomenclature, and
1101 sequence characteristics in the genomics era. *Insect biochemistry and molecular biology* **40**, 189-
1102 204.
1103 **Wong, L. L. and Adler, P. N.** (1993). Tissue polarity genes of Drosophila regulate the subcellular location
1104 for prehair initiation in pupal wing cells. *J Cell Biol* **123**, 209-221.
1105 **Yabe, T., Yamada-Okabe, T., Nakajima, T., Sudoh, M., Arisawa, M. and Yamada-Okabe, H.** (1998).
1106 Mutational analysis of chitin synthase 2 of Saccharomyces cerevisiae. Identification of additional
1107 amino acid residues involved in its catalytic activity. *Eur J Biochem* **258**, 941-947.
1108 **Zhang, X. and Zhu, K. Y.** (2013). Biochemical characterization of chitin synthase activity

1109 and inhibition in the African malaria mosquito, Anopheles

1110 gambiae. *Insect science* **20**, 158-166.
1111 **Zimoch, L. and Merzendorfer, H.** (2002). Immunolocalization of chitin synthase in the tobacco
1112 hornworm. *Cell Tissue Res* **308**, 287-297.

1113

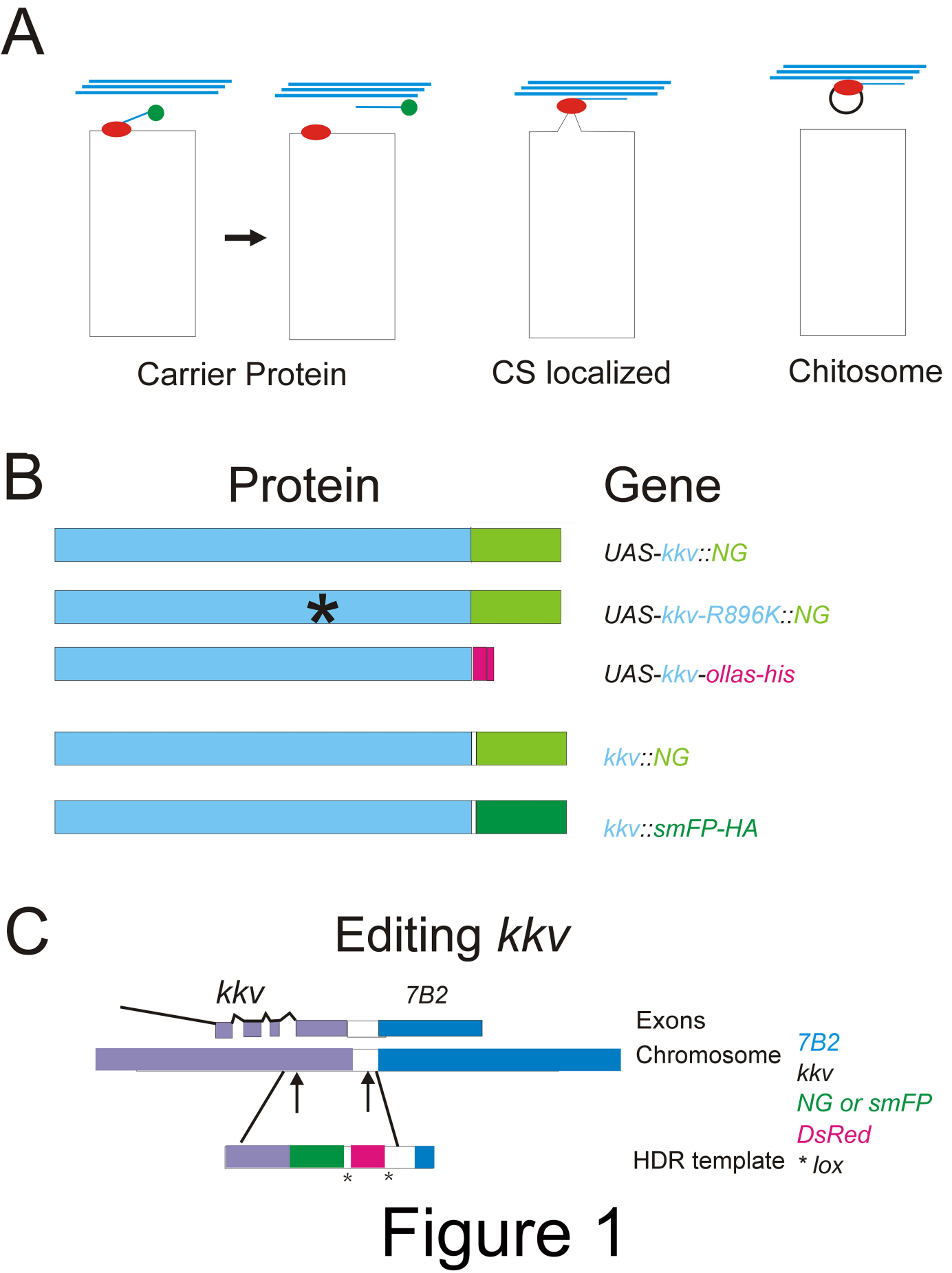
A
Carrier Protein
CS localized
Chitosome
B
Protein
Gene
UAS-kkv::NG
UAS-kkv-R896K::NG
UAS-kkv-ollas-his
kkv::NG
kkv::smFP-HA
C
Editing kkv
kkv
7B2
Exons
Chromosome
7B2
kkv
NG or smFP
DsRed
HDR template
* lox
*
*

Figure 1

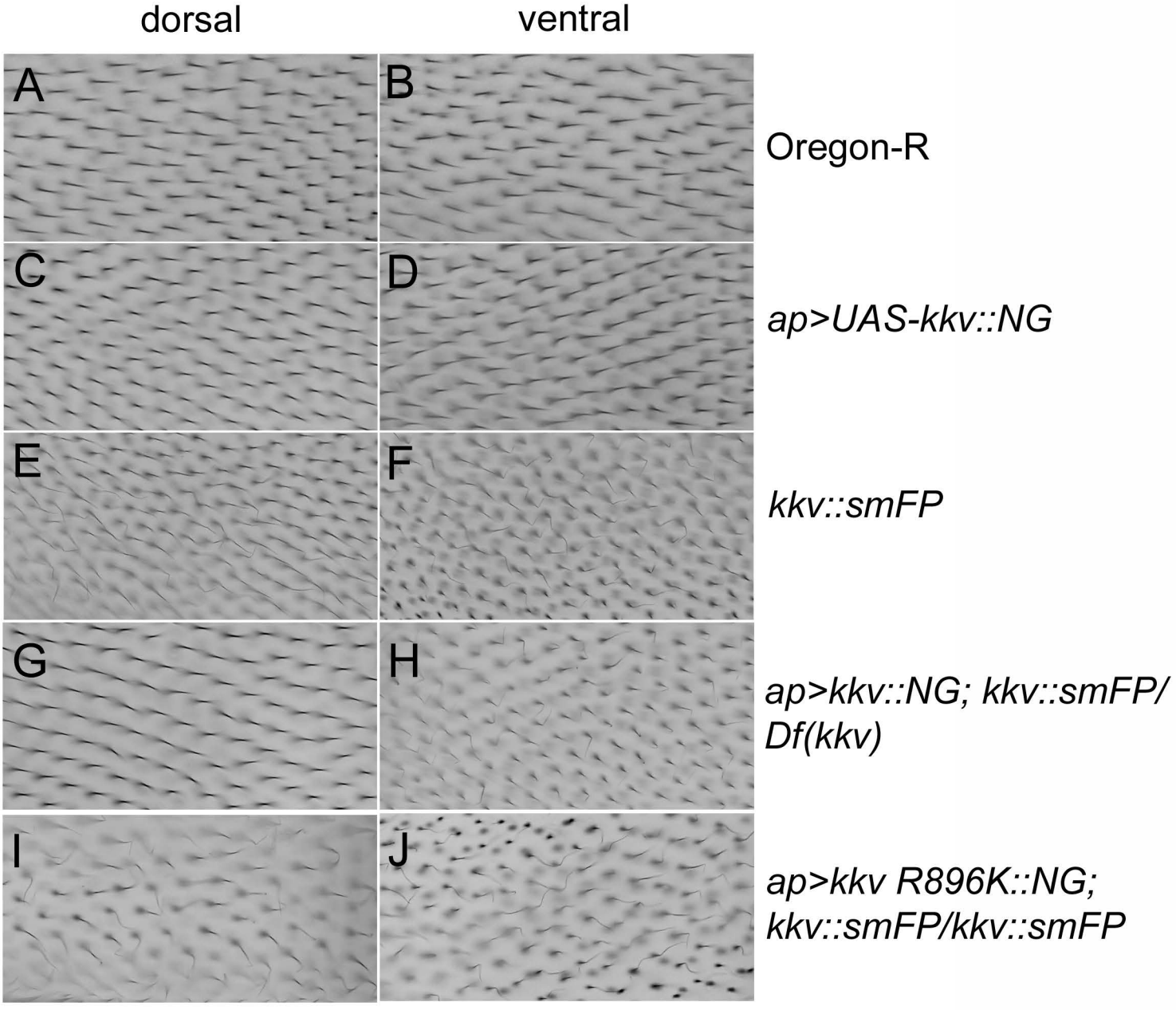
dorsal
ventral
A
B
Oregon-R
C
D
ap>UAS-kkv::NG
E
F
kkv::smFP
G
H
ap>kkv::NG; kkv::smFP/
Df(kkv)
I
J
ap>kkv R896K::NG;
kkv::smFP/kkv::smFP

Figure 2

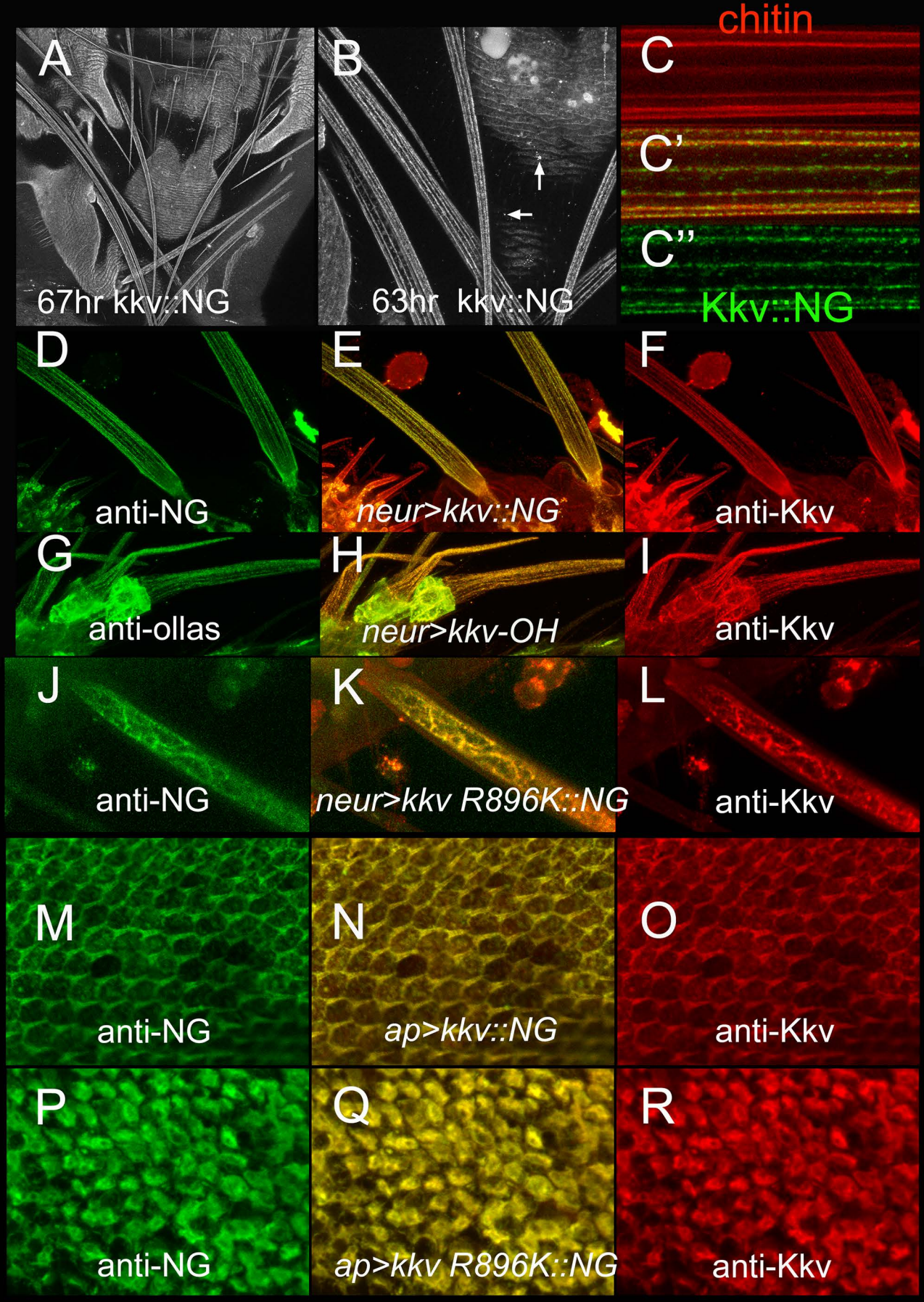
A
67hr kkv::NG
B
63hr kkv::NG
chitin
C
C'
C''
Kkv::NG
D
anti-NG
E
neur>kkv::NG
F
anti-Kkv
G
anti-ollas
H
neur>kkv-OH
I
anti-Kkv
J
anti-NG
K
neur>kkv R896K::NG
L
anti-Kkv
M
anti-NG
N
ap>kkv::NG
O
anti-Kkv
P
anti-NG
Q
ap>kkv R896K::NG
R
anti-Kkv

Figure 3

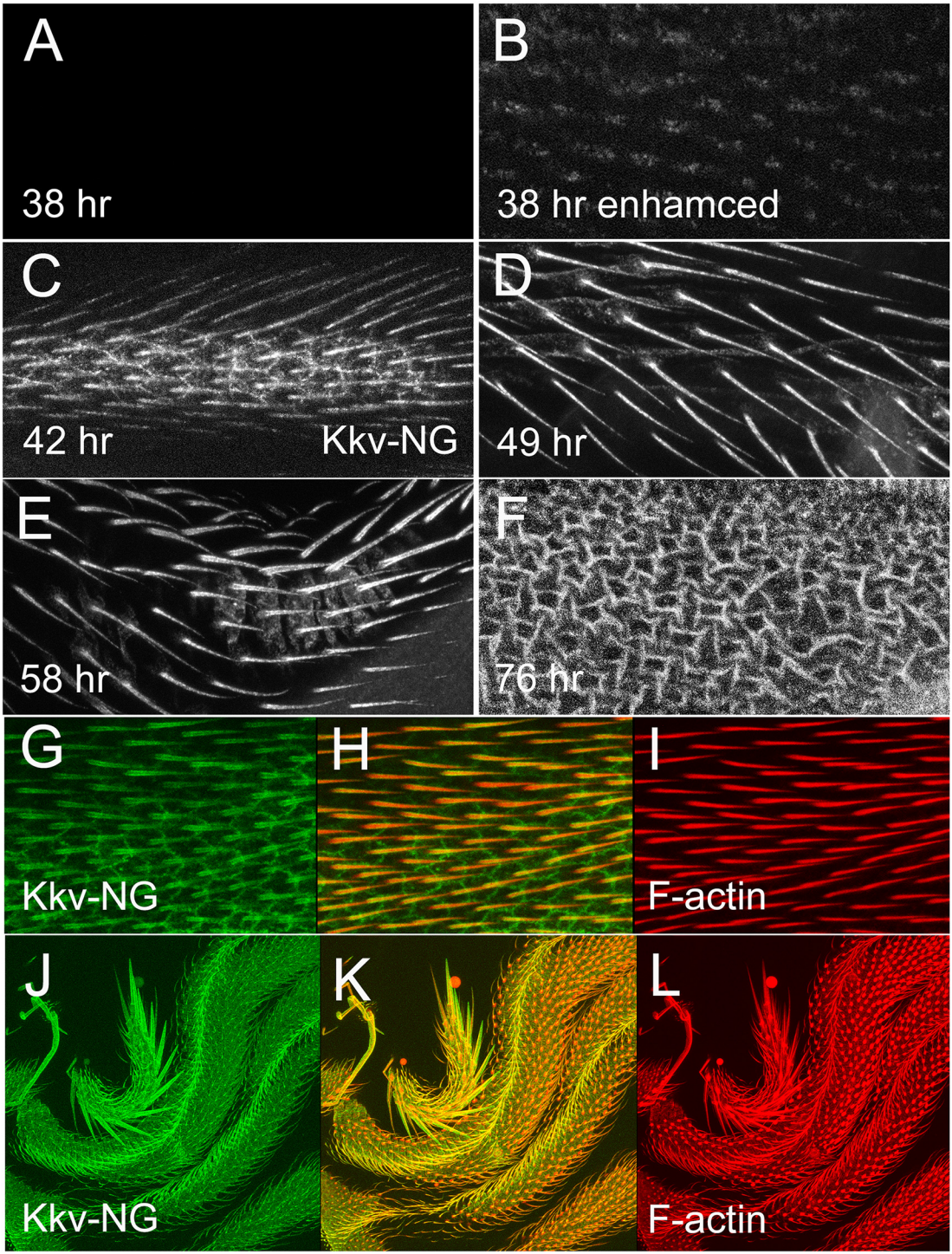
A
38 hr
B
38 hr enhamced
C
42 hr
Kkv-NG
D
49 hr
E
58 hr
F
76 hr
G
Kkv-NG
H
I
F-actin
J
Kkv-NG
K
L
F-actin

Figure 4

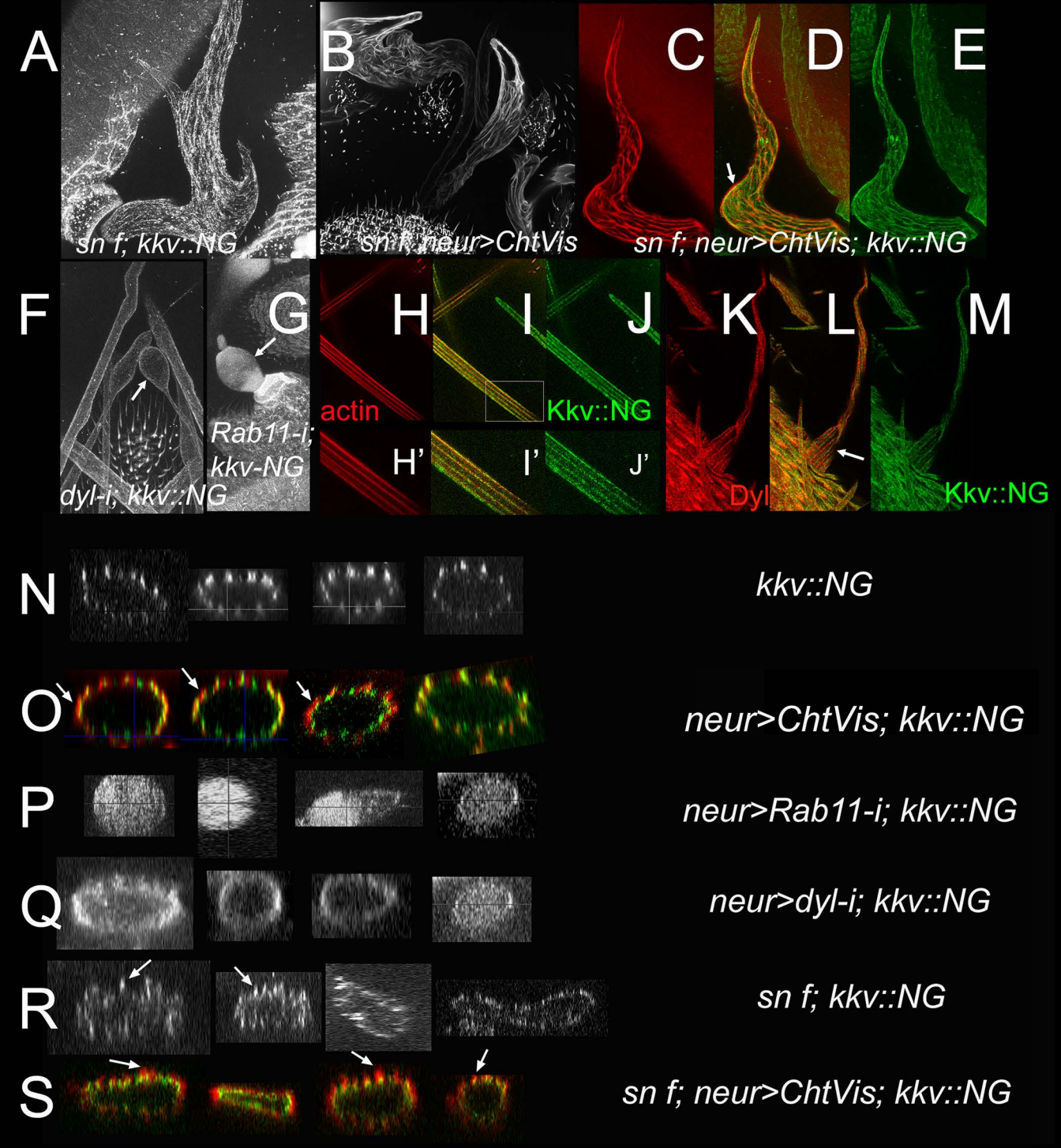
A
B
C
D
E
sn f; kkv::NG
sn f; neur>ChtVis
sn f; neur>ChtVis; kkv::NG
F
G
H
I
J
K
L
M
dyl-i; kkv::NG
Rab11-i;
kkv-NG
actin
Kkv::NG
H'
I'
J'
Dyl
Kkv::NG
N
kkv::NG
O
neur>ChtVis; kkv::NG
P
neur>Rab11-i; kkv::NG
Q
neur>dyl-i; kkv::NG
R
sn f; kkv::NG
S
sn f; neur>ChtVis; kkv::NG

Figure 5

A

anti-NG | anti-ollas | anti-Kkv-m | anti-Kkv-a | anti-Kkv-P2

PBST

PBS

ptc>kkv::NG | *ptc>kkv::OH*

B

Kkv

0 200 400 600 800 1000 1200 1400 1600

Predicted TMD

Antibody Probes

M A P2 C

Figure 6

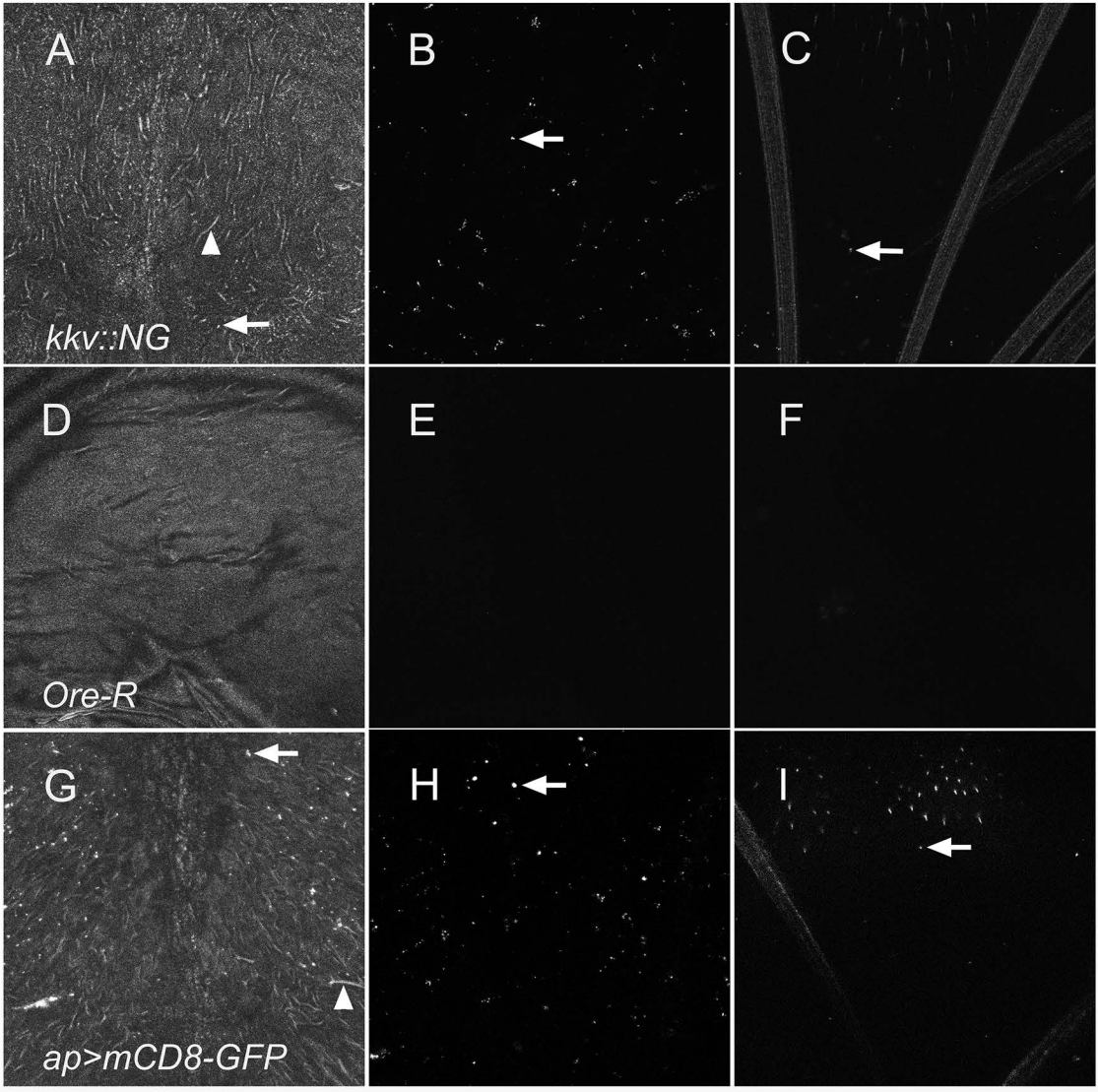

Figure 7

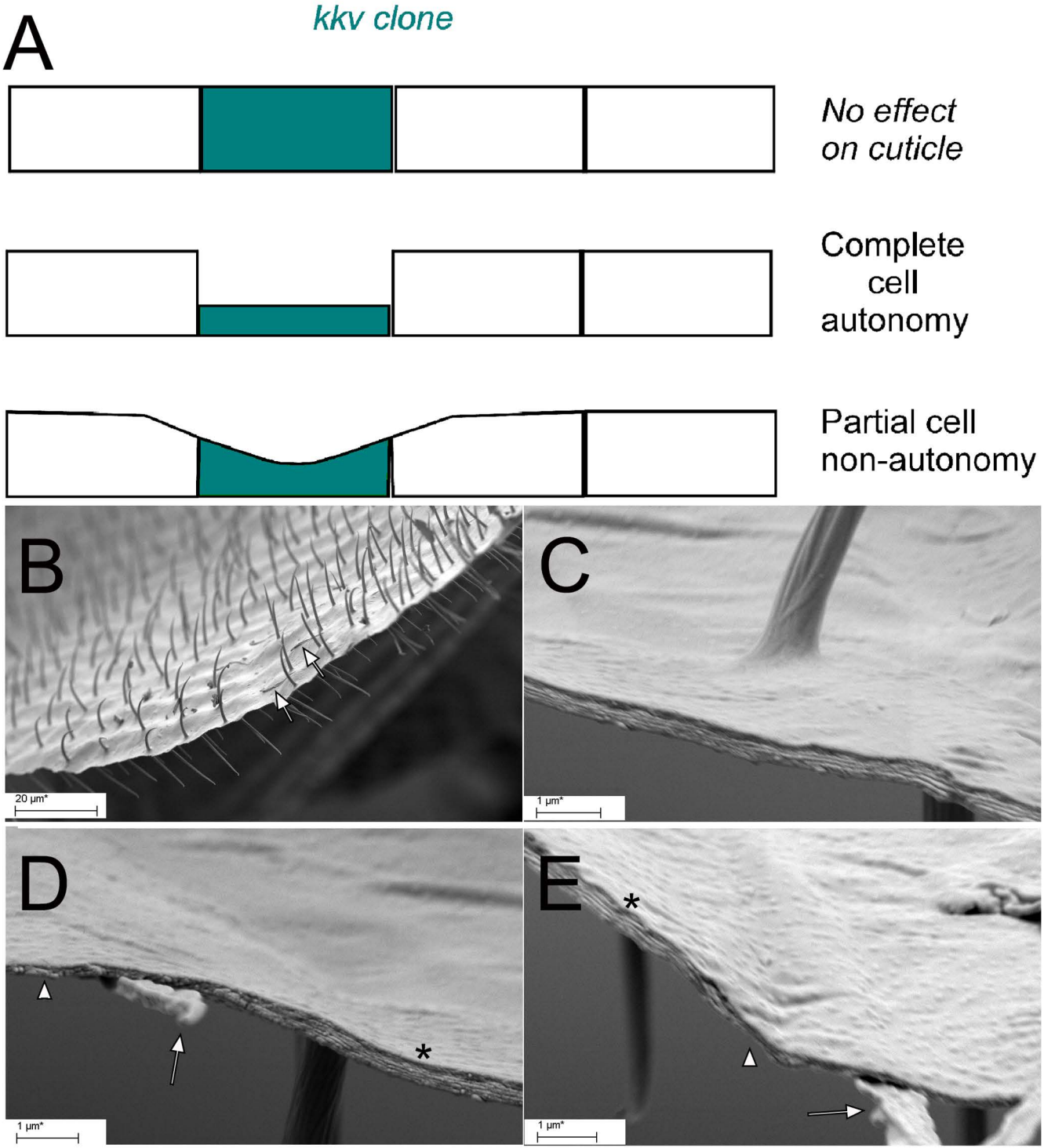
A
kkv clone
No effect on cuticle
Complete cell autonomy
Partial cell non-autonomy
B
20 µm*
C
1 µm*
D
1 µm*
E
1 µm*

Figure 8